3-24-2016

# The Efficacy of Implementing a Small, Low-Cost, Real Time Kinematic GPS System into a Small Unmanned Aerial System Architecture

Kevin J. Hendricks


# THE EFFICACY OF IMPLEMENTING A SMALL, LOW-COST, REAL TIME KINEMATIC GPS SYSTEM INTO A SMALL UNMANNED AERIAL SYSTEM ARCHITECTURE

THESIS

Kevin James Hendricks, Captain, United States Air Force

AFIT-ENV-MS-16-M-157

**DEPARTMENT OF THE AIR FORCE**
**AIR UNIVERSITY**

***AIR FORCE INSTITUTE OF TECHNOLOGY***

**Wright-Patterson Air Force Base, Ohio**

AFIT-ENV-MS-16-M-157

# THE EFFICACY OF IMPLEMENTING A SMALL, LOW-COST, REAL TIME KINEMATIC GPS SYSTEM INTO A SMALL UNMANNED AERIAL SYSTEM ARCHITECTURE

THESIS

Presented to the Faculty

Department of Systems Engineering and Management

Graduate School of Engineering and Management

Air Force Institute of Technology

Air University

Air Education and Training Command

In Partial Fulfillment of the Requirements for the

Degree of Master of Science in Systems Engineering

Kevin James Hendricks, BS

United States Air Force

March 2016

AFIT-ENV-MS-16-M-157

**THE EFFICACY OF IMPLEMENTING A SMALL, LOW-COST, REAL TIME KINEMATIC GPS SYSTEM INTO A SMALL UNMANNED AERIAL SYSTEM ARCHITECTURE**

Kevin James Hendricks, BS
Captain, USAF

Committee Membership:

Dr. David R. Jacques
Chair

Dr. John M. Colombi
Member

Dr. Sanjeev Gunawardena
Member

**Abstract**

Along with the growing uses for small unmanned aerial systems (UAS) within the Department of Defense (DoD), is the utility of small UAS within the civilian market is also increasing. This has led to significant research and development on small UAS subsystems by the commercial market. The focus of this research is characterizing and investigating the application considerations of a small, low-cost real time kinematic (RTK) GPS receiver system. Work was also accomplished to characterize the accuracy and precision of the commonly used GPS receiver subsystem in small UAS to show the increased utility of the RTK GPS system. The results show that in a static environment, the RTK GPS system outperforms the commonly used standalone GPS receiver by a factor of 100 in two- and three-dimensional precision. However, the results from the tests involving a moving platform exposed several limitations which can degrade the precision of the RTK GPS system to precision values achievable by a standalone GPS receiver. These limitations do not inhibit the RTK GPS system's ability to perform its primary intended purpose, and can be mitigated through proper integration and application selection of the system. It is recommended that the Air Force Institute of Technology continue to use the investigated RTK GPS system as a ground truth source while proving other navigation technologies for UAS flight.

*To my wife, parents and grandparents*

## *Table of Contents*

## List of Figures

## List of Tables

# 1. INTRODUCTION

This research describes the investigation of the application and characterization of commercially-available, low-cost technology to increase the geolocation accuracy of small unmanned systems. The primary goal of the research was to characterize a low-cost system capable of providing an increase in geolocation accuracy from 3 meters to within 10 centimeters. This characterization will provide insight into additional applications for which the unmanned system could be used and showcase the efficacy of using the low-cost hardware versus a higher-cost system.

## Problem Background

Unmanned Aerial Vehicles (UAVs) or Unmanned Aerial Systems (UASs) have been in use by the Department of Defense, or predecessor departments, since the earliest days of flight [13]. Although not as successful as the recent unmanned systems, these early UAVs gave engineers insight into the system level requirements that engineers have been improving upon ever since. An example of one of these early systems was a small group of stripped-down B-17s during WWII, called Operation Aphrodite. Commanded by Major General James H. Doolittle, the B-17s were stripped of nearly 12,000 pounds of flight hardware, including armor, seats and guns, to make room for 18,000 pounds of high explosives [13]. Communications system failures between the aircraft and the ground control station forced the program to be cancelled after the flights yielded only one success out of eight missions. This relatively unsuccessful program, however, paved the way for programs such as the Global Hawk and Predator B programs, which have shown great utility during global military operations over the past 15 years. Along with the growth in the government's use on unmanned systems, the number of UASs employed by hobbyists has also increased [8].

Along with the research and development conducted by government organizations, hobbyists have become interested in adding levels of autonomy to remote control (RC) aircraft. This has led to the miniaturization of flight hardware and the mass production of traditionally cost-prohibitive hardware items. On primary example of this is the key piece of hardware to be investigated by this thesis, is a Real-Time Kinematic (RTK) Global Positioning System (GPS) receiver. The system uses advanced, resource-intensive, algorithms and a real-time communications link to improve the geolocation accuracy. Before 2013, these systems were too large to fit on a small-UAS and highly cost-prohibitive to the hobbyist community, costing nearly $10,000. Due to the success of the non-government research community a complete system can now be purchased for less than 10% of that cost.

**Problem Statement**

Over the past 20 years, the use of unmanned systems has increased significantly as leaders realize the full suite of capabilities that unmanned systems present. Due to this increase in unmanned system application, there has also been a thrust in the research and development to further increase system capabilities. Many times, however, this new research is implemented in high-cost proprietary software and hardware or is classified. This precludes the cutting-edge research and development from being applied to materiel solutions quickly and at a low cost. Additionally, if the hardware or software is classified, then additional scrutiny is required to ensure that if the unmanned system is lost, an adversary could not reverse engineer or exploit the technology for their own use. Due to these limitations, the Air Force Institute of Technology has had numerous research projects focusing on the design and implementation of low-cost, off-the-shelf, autonomous vehicle systems over the past eight years.

The current research will focus on evaluating the efficacy of implementing commercially available RTK GPS hardware and software on a low-cost, off-the-shelf vehicle. Specifically, the research will characterize the Piksi RTK system developed by Swift Navigation to determine how well the system performs [22]. The Piksi RTK system advertises accuracies that have only previously been achievable at the cost of thousands to tens of thousands of dollars. This research will attempt to determine how well the Piksi RTK system, costing less than one thousand dollars, performs as advertised. The research will also suggest potential applications for the system.

The navigation system is one key piece of the architecture for aircraft in general. The widely used, open-source solution for geolocation leverages existing Global Navigation Satellite Systems such as the United States' Global Positioning System (GPS). The issue with implementing standard GPS receivers is that for some applications, the accuracy of a standalone GPS receiver, which is on the order of several meters, is not sufficient. Since the initial operating capability of the GPS constellation has been achieved, research has been conducted to attempt to refine the accuracy and precision of the position solutions achieved via GPS. This refining of the position solution has come at the cost of increased processing required which in turn leads to higher cost receiver units.

The higher accuracy and precision units have several applications for the Department of Defense (DoD). These include aerial surveillance, formation flight of UAS, and potentially surveying land for civil uses. In addition to applications for the DoD, a high accuracy and precision navigation solution is also utilized by agriculturalists. Large farms are now equipping tractors with GPS units to aid with planting and spraying. This research will provide limitation and recommendations for the application of the low-cost RTK GPS system being investigated.

## Research Objective

The objective of the research will be to evaluate the efficacy of implementing a COTS-GPS technology onto a COTS vehicle to demonstrate how a system can be retrofitted to increase the geolocation accuracy. The research will also provide suggestions on additional applications that the increased geolocation accuracy will allow the unmanned systems to perform.

## Investigative Questions

The research contained within this thesis set out to answer a set of research questions in order to fully answer the research topic:

- What is the accuracy of the current hobbyist hardware configuration?
- How can the RTK-GPS system be implemented into existing UAS architectures?
- How accurate and precise are the low-cost RTK systems?
- What are the limiting factors associated with the low-cost RTK system versus the traditional RTK systems?

## Scope of Research

Available to the hobbyist community are a vast array of technology that has yet to be fully characterized by the engineering or scientific community. The scope of this research was to characterize the performance of the Piksi RTK system produced by Swift Navigation.

Although the Piksi is not the first RTK-GPS system small enough to be capable of being integrated on a small UAS, it is one of the first to be priced at a level that makes it available to the high-end hobbyist. The research will focus on substantiating the claims made by the developer and demonstrate some potential applications for the increased level of geolocation accuracy.

## Methodology

There is not a recognized standard for characterizing RTK GPS receivers; therefore, characterizing the system will be done relative to high-cost components available for use at AFIT. To answer the investigative question, "What is the accuracy of the current hobbyist hardware configuration?", a short baseline test will be conducted. The remaining investigative questions will be answered by evaluating the Piksi RTK system. Testing of the Piksi will be done in three segments. First a zero-baseline test will be conducted in order to determine the accuracy of the receiver with and without the RTK algorithms. Next, the DGPS accuracy will be characterized relative to a high-accuracy differential system. Finally, integration tests will be conducted to show the utility of the Piksi RTK system on a small UAS.

## Definitions

Throughout the thesis, there are several terms the researcher will use frequently. These terms include: small-UAV and low-cost. Since each of these terms will have different meanings to different communities, the terms are defined below.

For this research, a small-UAV will be used to describe a UAV that is below the weight threshold of 20 pounds, has a maximum ceiling less than 1,200 feet and flies at speeds less than 100 knots. These limits were determined so that they are in-line with Group 1 of the UAS Groups as defined by the United States Air Force [6]. When the term low-cost is used it will refer to a total hardware and software costs less than $5,000 in 2016 U.S. dollars. This threshold is somewhat arbitrary but was chosen at that level to showcase the utility of the low-cost COTS technology, which is being used by the hobbyist community.

## Assumptions & Limitations

The primary assumption of the research is that neither the 915 MHz, the frequency utilized by the communication subsystem, nor the L1 GPS frequency is being interfered with. The 915 MHz and L1 GPS signals are critical to the employment of the vehicles, without which, testing cannot be accomplished.

One other fundamental assumption is that the Piksi receiver units being characterized are a good representative of other Piksi receivers and are not defective. The results will show that this is very likely not the case, but this assumption is still required to account for factory defects.

One final limitation is that at some point during the research the configuration of the Piksi firmware needed to be kept constant. Since the Piksi is very new to the market, many improvements were still being made to the firmware running onboard the receivers. Swift Navigation breaks up the firmware into two files. The STM software refers to the software running on the microcontroller imbedded on the Piksi board and NAP refers to the software running on the field programmable gate array (FPGA). The firmware revisions used for this research were the STM version 0.20 and NAP version 0.15.

## Summary

The ever-improving technology of COTS hardware being implemented by RC-hobbyists is showing greater and greater potential. This research will focus on characterizing one of these new pieces of technology and show how the technology can be implemented for applications that were not otherwise feasible at the price-point.

Subsequent chapters will provide more insight into the characterization of COTS geolocation systems. Chapter 2 will outline a background on how the GPS system is utilized to

obtain high-accuracy position solutions, followed by a brief industry survey, and a discussion of relevant previous work that has been done in this area of study. Chapter 3 will explain in detail the methodology used to characterize the geolocation systems being investigated. Chapter 4 will present the results of the experiments. Finally, in Chapter 5, conclusions regarding the research will be made along with suggestions for potential applications and further research.

# 2. BACKGROUND

Within this section, a more in-depth background into topics relevant to this thesis will be introduced. First, an overview of the GPS system, and how the system is used to generate accurate position solutions, is discussed. Then, a brief industry survey of the commercially-available GPS receiver options will be addressed to demonstrate the apparent price gap between traditional RTK-GPS systems and the low-cost system discussed in this thesis. Once it is clear which components are to be used, a review of applicable literature will be detailed including recent research on RTK-GPS systems.

## GPS Overview

Developed in the late 1960s and operational in the early 1980s, the GPS constellation has become the industry standard for the geolocation of manned and unmanned aircraft. The GPS system can be broken up into three segments: user, control and space. The space segment consists of the constellation of approximately 30 space vehicles (SV) contained within six orbital planes, each of which is inclined 60 degrees with respect to the equatorial plane at an altitude of around 12,550 miles [10]. The control segment includes a master and alternate control station, 12 command and control antennas, and 16 monitoring sites [10]. Lastly, the GPS-user segment consists of all of the GPS receivers operated by end users. Collectively, the three segments of the GPS system provide the end user with continuous position and time measurements. The next section will provide a brief background on how the measurements are formed.

### GPS Location Measurements

Currently, there are three frequency bands used by the GPS constellations: L1, centered at 1575.42 MHz; L2, centered at 1227.60 MHz; and L5, which is centered at 1176.45 MHz [3].

Since most low-cost receivers use only the L1 frequency, this section will focus on how position solutions are garnered from a single frequency.

Location measurements, or solutions, may be obtained using two primary methods. The first method uses the Coarse/Acquisition (C/A) code to distinguish the time between when the code sequence was transmitted by the SV to the time that it was received on the ground. Since each satellite has a specific C/A code, referred to as its pseudorandom noise (PRN) code, it is possible to distinguish the amount of time the signal took to reach the user receiver from each of the visible SVs. The time is then multiplied by the speed of light, approximately 30 million meters per second, to calculate the range from each satellite. The C/A code is a 1023-bit sequence, with a chipping frequency of $1.023 \times 10^6$ chips per second, which allows the code to repeat itself every millisecond [3]. This high-repeat rate allows for ground receivers to lock onto the signal quickly. Also transmitted on the L1 frequency, but on the orthogonal carrier phase with respect to the C/A code, is the Precision (P) code [3]. The P-code was designed for high-accuracy military applications. As such, it is encrypted with what is referred to as Y-code to prevent spoofing. This combined signal is referred to as P(Y)-code. Along with being encrypted, the P(Y)-code is a $10^{14}$ bit sequence which makes it extremely difficult to lock onto without accurate knowledge of absolute time to within a few microseconds. For this reason most P(Y) code receivers acquire and track the C/A code signal before handing over to P(Y) code tracking [3].

The measurements received from tracking the C/A code is commonly referred to as the pseudorange. The range from each of satellites is commonly referred to as pseudoranges due to the measurement of true range being obscured by an unknown error in the receiver clock. This requires four satellites to be visible to the GPS receiver for accurate three dimension absolute

position to be determined instead of three. There are also several other large errors such as the errors affecting the range measurement. The equation for pseudorange is shown in ( 2-1 ) **[**24**]**.

$$\rho = r + c[\delta t_u - \delta t^s] + I_\rho + T_\rho + mp + v \qquad (2\text{-}1)$$

where:

$\rho = pseudorange\ (m)$

$r = true\ range\ (m)$

$c = speed\ of\ light\ \left(299792458\frac{m}{s}\right)$

$\delta t_u = receiver\ clock\ error\ (s)$

$\delta t^s = satellite\ clock\ error\ (s)$

$I_\rho = measurement\ delay\ due\ to\ ionosphere\ (m)$

$T_\rho = measurement\ delay\ due\ to\ troposphere\ (m)$

$mp = measurement\ delay\ due\ to\ multipath\ (m)$

$v = receiver\ noise\ (m)$

Absolute three-dimensional position solutions are obtained by computing pseudorange measurements from at least four SVs. For more information regarding the error terms and mitigations for those terms, a full explanation can be found in [15].

Instead of using the C/A or P-code to determine distances from the SVs, the other method for determining position is carrier-phase tracking. After locking onto the PRN code from each of the visible SVs, carrier phase measurements track the accumulated Doppler of the carrier frequency [15]. Given that the L1 carrier frequency is about 1540 times greater than the C/A-code chipping frequency, a higher-precision measurement is obtained, which in-turn corresponds to higher-accuracy position solutions. The high accuracy leading to a high precision is due to the errors associated with GPS signals being normally distributed around the true position. The

downside, however, is that some additional post-processing of the measurement is required in order to determine the distance – since the carrier phase measurement is in units of cycles. The equation for the carrier-phase measurement is shown in ( 2-2 ).

$$\varphi = \frac{1}{\lambda}\left[r + c(\delta t_u - \delta t^s) - I_\rho + T_\rho + mp + v\right] + N \qquad (2\text{-}2)$$

Where r, c, $\delta t_u$, $\delta t^s$, I, T are defined in ( 2-1 ).

$$\varphi = Carrier\ phase\ measurement\ (cycles)$$
$$\lambda = carrier\ wavelength\ \left(\frac{m}{cycle}\right)$$
$$N = integrer\ ambiguity(number\ of\ cycles)$$

As shown in Equation ( 2-2 ), the equation used for carrier phase tracking is very similar to Equation ( 2-1 ), which is used for pseudorange measurements. There are, however, two primary differences in the equations. The first is the effect that the ionosphere has on the measurement. This is shown by the $-I_\rho$ in ( 2-2 ) versus the $+I_\rho$ in Equation ( 2-1 ). The other, more troublesome, difference is that ( 2-2 ) is in terms of cycles and requires the ambiguity term, N, be resolved, before determining the distance between the receiver and the SV. There are several techniques that have been developed for resolving the integer ambiguity. One popular method for resolving the ambiguities is called the Least Squares Ambiguity Decorrelation Adjustment (LAMBDA) method. A full derivation of the LAMBDA method can be found in [26].

Differential GPS

One of the primary methods used to reduce the amount of error in the GPS position solution is using differential GPS (DGPS). DGPS works to reduce spatially correlated errors by calculating the difference between the known range and the pseudorange, which is used by the

receiver to calculate a position solution. It is important to note that while the spatially correlated errors, such as troposphere and ionosphere delays are reduced, the non-spatially correlated errors such as measurement noise and multipath, are increased. This is a good tradeoff, however, because the spatially-correlated errors are a much larger contributor to the total error than the non-spatially-correlated errors. The following two sections will detail single- and double-difference GPS.

*Single Differencing*

Single differencing involves using the differential between two receivers in view of the same SV. Figure 2-1 shows a schematic of how single difference works between satellite *a* and receivers *x* and *y*.

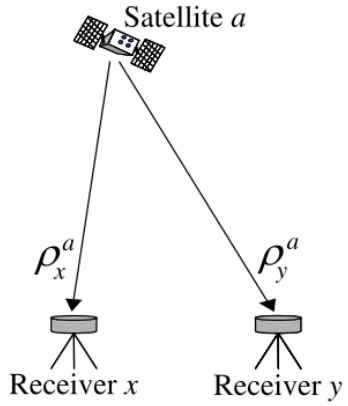


Figure 2-1: Single Difference Schematic [25]

The difference between the pseudorange of receiver *x* relative to satellite *a* and receiver *y* relative to satellite *a* is shown in ( 2-3 ).

$$\Delta\rho_{xy}^{a} = \rho_{x}^{a} - \rho_{y}^{a} \qquad (2\text{-}3)$$

where:

$\Delta\rho_{xy}^{a} = single\ difference\ measurement\ (m)$

$$\rho_x^a = pseudorange\ from\ satellite\ a\ to\ receiver\ (m)$$

$$\rho_y^a = pseudorange\ from\ satellite\ a\ to\ receiver\ y\ (m)$$

By substituting ( 2-1 ) into ( 2-3 ), each of the terms in the pseudorange equation becomes differential terms as shown in ( 2-4 ).

$$\Delta\rho_{xy}^a = \Delta r_{xy}^a + \Delta c\delta t_{u,xy}^a - \Delta c\delta t_{xy}^{s,a} + \Delta I_{xy}^a + \Delta T_{xy}^a + \Delta mp_{xy}^a + \Delta v_{xy}^a \qquad (2\text{-}4)$$

As noted in the introduction to this section, the satellite clock term is completely eliminated since that term is common in between the two receivers. The ionosphere and troposphere terms are decreased significantly, if the distance between the two receivers is small. The multipath and measurement noise terms increase by a factor of $\sqrt{2}$. Following the same steps as were conducted for the pseudorange equations, an equation for single-difference carrier phase measurements is shown in ( 2-5 ).

$$\Delta\varphi_{xy}^a = \frac{1}{\lambda}\left[\Delta r_{xy}^a + \Delta c\delta t_{u,xy}^a - \Delta c\delta t_{xy}^{s,a} - \Delta I_{xy}^a + \Delta T_{xy}^a + \Delta mp_{xy}^a + \Delta v_{xy}^a\right] + \Delta N_{xy}^a \qquad (2\text{-}5)$$

By implementing single difference DGPS, the accuracy of C/A code measurements is improved from 10 meters to about 1 meter. Double differencing can be applied for an even greater improvement in position accuracy.

*Double Differencing*

In order to reduce the errors even greater than what is possible using single differencing, the double difference method can be implemented. Double differencing relies on two receivers receiving information from two SVs simultaneously. If this condition holds, then the receiver-error term is eliminated. Figure 2-2 shows a schematic for double differencing.

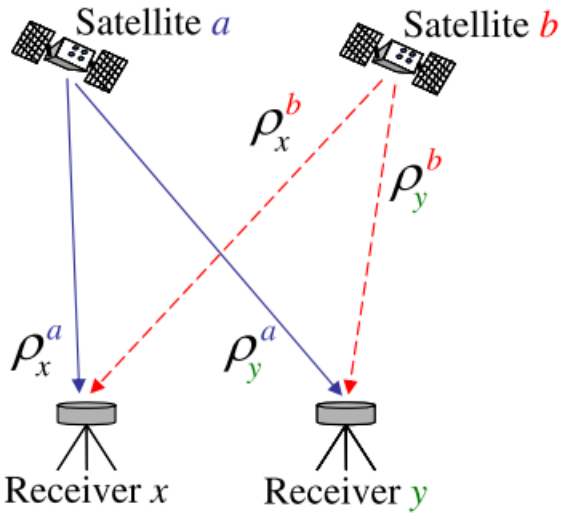


Figure 2-2: Double Difference Schematic [25]

Double differencing is very similar to single differencing. The distinction is that, whereas single difference uses the pseudorange or carrier phase measurements as inputs, double differencing uses the single difference of the pseudorange as inputs. Equation ( 2-6 ) is the formula used to obtain the correction.

$$\Delta\nabla\rho_{xy}^{ab} = \Delta\rho_{xy}^{a} - \Delta\rho_{xy}^{b} \qquad (2\text{-}6)$$

where:

$\Delta\nabla\rho_{xy}^{ab} = double\ difference\ of\ receivers\ x\ and\ y\ relative\ to\ satellites\ x\ and\ y\ (m)$

$\Delta\rho_{xy}^{a} = \ single\ difference\ of\ receivers\ x\ and\ y\ relative\ to\ satellite\ a\ (m)$

$\Delta\rho_{xy}^{b} = single\ difference\ of\ receivers\ x\ and\ y\ relative\ to\ satellite\ b\ (m)$

By combining ( 2-4 ) and ( 2-6 ) the double difference equation becomes:

$$\Delta\nabla\rho_{xy}^{ab} = \Delta\nabla r_{xy}^{ab} + \Delta\nabla I_{xy}^{ab} + \Delta\nabla T_{xy}^{ab} + \Delta\nabla mp_{xy}^{ab} + \Delta\nabla v_{xy}^{ab}\Delta\nabla \qquad (2\text{-}7)$$

The terms for ionosphere and troposphere are further reduced, the receiver clock error term is

eliminated, but the error contribution from multipath and noise are increased by a factor of 2 over the single C/A code tracking. Like single differencing, the method can also be applied to carrier phase measurements.

$$\Delta\nabla\varphi_{xy}^{ab} = \frac{1}{\lambda}\left[\Delta\nabla r_{xy}^{ab} - \Delta\nabla I_{xy}^{ab} + \Delta\nabla T_{xy}^{ab} + \Delta\nabla mp_{xy}^{ab} + \Delta\nabla v_{xy}^{ab}\right] + \Delta\nabla N_{xy}^{ab} \qquad (2\text{-}8)$$

By implementing double differencing with carrier phase measurements, position errors are in the range of 1-3 millimeters, when using high-end GPS equipment [24].

*Real Time Kinematics*

The high precision carrier phase measurements are utilized by the Piksi RTK algorithms to calculate a relative position of one receiver to the other. The RTK algorithms onboard the Piksi utilize the double differenced carrier phase measurements to solve for the integer ambiguity in near real time. The receiver pre-designated as the base receiver then sends its measured carrier phase to the mobile receiver. The processors onboard the mobile receiver then compare the carrier phase sent to it by the base receiver to the measured carrier phase from its own receiver. The comparison of the two carrier phase measurements along with information regarding the azimuth and elevation position of the GPS satellites allow the calculation of a baseline distance, or distance between the two receivers.

The position solutions output from the RTK algorithm are in a relative coordinate frame, typically centered at the base receiver location for simplicity, not an absolute coordinate frame. Absolute measurements can be obtained from the RTK algorithm if the location of the base receiver's antenna is known in the absolute coordinate frame. A coordinate frame transformation, as described in Chapter 3, can then be used to convert the relative baseline

positions to an absolute coordinate frame. This is the method used to characterize the accuracy and precision of the Piksi RTK system. De-facto

**GPS Receiver Industry Survey**

There are many COTS components available for implementing high-accuracy positioning [9]. However, many of these systems are either too large to fit into a small-UAS or they are above the threshold for considering the system low-cost. Within this section, a small trade study of the available technology is conducted in order to show the reader how the selected components' capabilities compare to industry-standard components.

The RC-industry de facto standard for providing accurate, absolute locations is the 3DR uBlox GPS with compass kit [1]. The 3DR kit is very low-cost, roughly $90, light-weight, and easily integrated with existing autopilots such as the APM or Pixhawk [1]. These autopilots allow, among other features, the capability of waypoint following for off-the-shelf small-RC aircraft. The drawback to using this component for high-accuracy geolocation is that the system is not equipped with an on-board processor that will allow for carrier phase ambiguity resolution or DGPS. As such, the position solution accuracy will be limited by the pseudorange measurement accuracy.

On the other end of the cost spectrum is the SBG Systems Ellipse-D. The system has a much higher level of accuracy relative to the 3DR component. This is made possible by onboard processing to conduct the carrier phase ambiguity resolution, as well as double differencing GPS. The system is also capable of receiving signals on both the L1 and L2 frequencies, which allows for a more accurate assessment of the error induced by the signal passing through the ionosphere and, thus, a more precise measurement [15]. However, the primary drawback to the system in

regard to this research is the high cost. At $14,000 each at the time this paper was written, the system is well above the cost threshold defined in Chapter I.

In the middle of the cost-spectrum are two high-accuracy GPS receivers that have become available within the past three years: the Swift Navigation Piksi and the Emlid Reach. The Swift Navigation Piksi (Piksi) is an out-of-the-box capable RTK GPS system originally developed using money from a Kickstarter campaign [14]. Since the makers of the system are relatively new to the game, the open-source software running on the field-programmable gate array (FPGA) is constantly being tweaked to allow for faster GPS lock and increasing the algorithm's accuracy. The price of the system is around $1K for two receivers, allowing the full UAS to remain below the cost threshold. Piksi uses double differencing of the carrier phase measurements to send error corrections from a base station, with known geocoordinates, to a rover vehicle. Since the system relies on the user to input the absolute position of the base receiver, the accuracy achieved is only in terms of a local coordinate system centered on the base receiver. The relative accuracy of the system is advertised to be within 10 centimeters. Verifying this value is a goal of this research and will be discussed further in Chapters 3 and 4. The Piksi system was the lone system at the lower end of the RTK cost spectrum, until the Emlid Reach system was introduced in mid-2015.

The Emlid Reach (Reach) system is very similar to the Swift Navigation Piksi, in that it is marketed as an out-of-the-box, low-cost RTK GPS solution [7]. Other than being about half the cost and half the size of the Piksi, the main disparity between the two systems is that the Reach has an imbedded nine degree of freedom inertial measurement unit (IMU) and is compatible with wireless networking out of the box. The imbedded IMU is a key feature sets the Reach apart from the Piksi system. If integrated into the system correctly, the IMU allows the

aircraft to sense its orientation. The outputs can also be fed directly into the imbedded Intel processor within the Reach, to further enhance the positional accuracy of the system. The wireless network compatibility allows for the system to receive corrections from space and land based correction services in real-time.

As more and more small UAS users begin to adopt RTK GPS systems for use in the field, it is very likely that the number of companies involved will continue to grow. The purpose of this research is not to characterize all of the low-cost RTK systems; rather, the purpose is to show how effective one of these systems is relative to a high-cost system.

## Literature Review

To ensure that this thesis is not merely a duplication of the effort of previously completed research, a comprehensive literature review was conducted. Within each subsection, relevant articles and thesis papers are reviewed; the areas where they leave off and this research picks up are annotated. Within the past 10 years, AFIT has conducted several research projects designing and implementing high-accuracy, dynamic GPS receiver systems. That research will serve as the baseline regarding what is being done on the receiver side to allow for high-accuracy and what level of accuracy should be expected.

### AFIT Thesis Research

The thesis research completed by Major Christopher J. Spinelli in 2006, annotated the design, implementation and testing of a RTK GPS system. The primary focus of his research was the implementation of a novel approach for resolving the ambiguity associated with using the carrier phase measurements for the location solution [25]. Spinelli postulated a new method for determining the true set of ambiguity solutions from the set of candidate solutions, which was

determined using the LAMBDA method. Where traditional methods would pick the ambiguity solution based on the position solution with the lowest residuals, Spinelli implemented a least-square fit on the residuals over time. The true set of ambiguity solutions, he observed, would be the set which fit a linear curve with a near-zero slope and y-intercept. The erroneous sets would exhibit more parabolic quantities. Both ground and flight testing showed that the method Spinelli proposed resulted in lower mean radial spherical error (MRSE), or error in the three-dimensions, than the traditional approach. The static ground tests averaged a MRSE of 1.4 centimeters, while the mobile tests averaged 9.5 centimeters. This research demonstrated the high-accuracy positioning, when using a RTK GPS system. While this thesis will not attempt to improve upon the accuracy or robustness of Spinelli's position solution, it will show how a smaller, low-cost COTS component, such as the Piksi, compares to the system that Spinelli designed and implemented.

Commander Stephen J. Comstock attempted to implement a similar system to Spinelli. The primary difference was the integration platform. Whereas Spinelli's system was proposed for an automated aerial refueler, the goal of Comstock's research was to implement a high-accuracy system for UAS formation flight control [5]. Since the system was intended for a UAS, and not a larger manned platform, component size and weight were key considerations when selecting hardware. Comstock made up for the smaller component size by using a dual-frequency receiver, which was capable of tracking both the L1 and L2 signal. The dual-frequency receiver not only allowed for a more precise estimation of the ionosphere, but also allowed for Comstock to use the widelane measurement, or the difference between the carrier phase of L1 and L2. The addition of the widelane measurement allowed the ambiguity resolution routines to converge much faster than an ambiguity resolution routine using a single

frequency. The use of the widelane measurement will, however, decrease the final position solution accuracy since the widelane measurement wavelength is about four times longer than using the wavelength from the L1 or L2 signal [5]. Comstock realized this accuracy reduction. Although the convergence time of the algorithm was on the order of two seconds, measurement accuracy was 3.5 centimeters MRSE [5]. The research indicates that the addition of a second frequency can decrease the solution time for a high-accuracy measurement.

These two AFIT theses demonstrate the ability of highly-customized hardware and software to output a high-accuracy position solution. A review of the work being conducted outside AFIT was also included to give this literature review some breadth.

Industry RTK research

Several researchers have begun exploring the problem of implementing a low-cost, high-accuracy positioning system. Stempfhuber and Buchholz used a pair of low-cost uBlox receivers—similar to those used in the 3DR kit—and a set of open source algorithms, RTKlib, as a proof of concept [21]. They attached one receiver to a Lego Mindstorm NXT-model and the other fixed at a base station. The base station, with known reference position, would then send corrections over a Wi-Fi connection to the mobile receiver to allow for high-accuracy relative positioning. Although the accuracy of the solutions is not clear, Stempfhuber and Buchholz' research demonstrates the interest in developing a low-cost, high-accuracy positioning system.

Pilz et al. implemented the system described by Stempfhuber and Buchholz onto a small quadrotor UAS [19]. The goal of their research was to optimize the ability of a UAS to closely follow a pre-defined route. Implementing the lower-end, single frequency receivers and RTK algorithms used by Stempfhuber and Buchholz, Pilz et al. demonstrated a MRSE of 20

centimeters [19]. While the error is drastically higher than the error realized by the two AFIT theses discussed, it demonstrates the ability of a low-cost, single-frequency system. While the AFIT theses show the high-end accuracy that the tested COTS component will likely not achieve, the COTS component should be within the system accuracy studied by Pilz et al.

**Summary**

This chapter has presented the background material required for an understanding of the remaining thesis chapters. This chapter started with an overview of the GPS system, as well as the techniques used to obtain up to millimeter-level accuracy. Then, a brief industry survey was discussed in order to show how the COTS system being investigated fits within the GPS market. Finally, a literature review of both AFIT theses and non-AFIT academic research was conducted to show how the results of this research will help propel the technology in this area. The following chapter will describe the methodology used to characterize the selected COTS RTK-GPS system, the Swift Navigation Piksi.

# 3. METHODOLOGY

This chapter addresses the method used to characterize and implement a representative low-cost RTK-GPS system, the Swift Navigation Piksi. There is not a recognized standard for characterizing RTK GPS receivers; therefore, characterizing the system will be done relative to high-quality, high-cost components available for use at AFIT. To answer the investigative question, "What is the accuracy of the current hobbyist hardware configuration?", a short baseline test will be conducted using the current standard GPS unit implemented with commercially available autopilots. The remaining investigative questions will be answered by evaluating the Piksi RTK system. Testing of the Piksi will be done in three segments. First a zero-baseline test will be conducted in order to determine the single point accuracy of the receiver. Next, the DGPS accuracy will be characterized relative to a high-accuracy differential system. Finally, integration tests will be conducted to show the utility of the Piksi RTK system on a small UAS.

**Coordinate Frame Transformation**

Standard GPS receivers are setup to output position solutions in degrees of latitude, degrees of longitude and height above ellipsoid in meters. It is difficult to interpret the results of simply comparing the difference between two solutions in degrees of latitude and longitude; therefore, a coordinate frame transformation is conducted. The coordinate frame transformation applied to this research allows the transformation of a set of test points in an absolute coordinate frame to a local-level coordinate frame with an origin to be specified by the researcher. The axes of the local level coordinate frame are distances from the origin in meters north, east and down.

The calculation of the distance between two points expressed in latitude, longitude and height can be done using the following equations.

$$p_e = \left(\frac{a}{(1 - e^2 \sin^{-1} \varphi)^{1/2}} + h\right) \cos \varphi \Delta\lambda$$

$$p_n = \left(\frac{a(1 - e^2)}{(1 - e^2 \sin^{-1} \varphi)^{3/2}} + h\right) \Delta\varphi \qquad (3\text{-}1)$$

$$p_u = \Delta h$$

where

$p_e = east\ position\ relative\ to\ local\ level\ coordinate\ frame\ (meters)$

$p_n = north\ position\ relative\ to\ local\ level\ coordinate\ frame\ (meters)$

$p_u = height\ relative\ to\ local\ level\ coordinate\ frame\ (meters)$

$\Delta\lambda = change\ in\ longitude\ relative\ to\ origin\ (radians)$

$\Delta\varphi = change\ in\ latitude\ relative\ to\ origin\ (radians)$

$\Delta h = change\ in\ height\ relative\ to\ origin\ (meters)$

$\varphi = latitude\ of\ center\ point$

$a = semi - major\ axis\ of\ Earth\ (6378.137\ km)$

$e = Earth\ eccentricity (0.0818191908426)$

Equation ( 3-1 ) was used extensively throughout the data analysis to determine the error from a known location.

**Error statistics**

The accuracy of the Piksi receiver was calculated using the two and three-dimensional versions of the root-mean square. The need to break apart the analysis of the two-dimensional statistics from the three-dimensional statistics is due to the known inaccuracy of GPS height measurements. The equation commonly used for the two dimensional and three dimensional

accuracy, denoted distance root mean square (DRMS) and mean radial spherical error (MRSE), are found in ( 3-2 ) and ( 3-3 ), respectively.

$$DRMS = \sqrt{\frac{\sum_{i=1}^{n}\left[\left(p_e^i\right)^2 + \left(p_n^i\right)^2\right]}{n}} \quad (3\text{-}2)$$

$$MRSE = \sqrt{\frac{\sum_{i=1}^{n}\left[\left(p_e^i\right)^2 + \left(p_n^i\right)^2 + \left(p_u^i\right)^2\right]}{n}} \quad (3\text{-}3)$$

where

$p_e^i = i^{th}\ east\ position\ relative\ to\ the\ true\ solution\ (meters)$
$p_n^i = i^{th}\ north\ position\ relative\ to\ the\ true\ solution\ (meters)$
$p_u^i = i^{th}\ height\ relative\ to\ the\ true\ solution\ frame\ (meters)$

The precision of the tested components were computed using the two- and three- dimensional versions for the standard deviation of a Gaussian function, denoted $\sigma_{2D}$ and $\sigma_{3D}$. These equations are found below in ( 3-4 ) and ( 3-5 ).

$$\sigma_{2D} = \sqrt{\sigma_e^2 + \sigma_n^2} \quad (3\text{-}4)$$

$$\sigma_{3D} = \sqrt{\sigma_e^2 + \sigma_n^2 + \sigma_u^2} \quad (3\text{-}5)$$

where

$\sigma_e = standard\ deviation\ of\ the\ p_e\ measurements$
$\sigma_n = standard\ deviation\ of\ the\ p_n\ measurements$
$\sigma_u = standard\ deviation\ of\ the\ p_u\ measurements$

In addition to the equations used to measure the accuracy and precision of the components, a limitation of the Piksi RTK system was uncovered during the testing resulting in the need to derive a metric. The metric, referred to as output reliability, is a measure of how

often the Piksi RTK system outputs a position solution at the desired interval. For a UAS, this measure should be very close to one to make sure that the system knows where the vehicle is located. Many autopilots within the UAS will enter into a failsafe mode if it senses that there is an issue with the GPS receiver. The output reliability metric gives a percentage of how many times throughout the test the time difference between the output of consecutive position solutions matches the specified output frequency. The MATLAB code used to calculate the output reliability can be found in the appendix.

**3DR Short Baseline Test**

The precision and accuracy of the current hobbyist GPS hardware, the 3DR GPS kit, was deduced by conducting a short baseline test. For this test the 3DR kit was placed at a known distance from a high accuracy GPS receiver. After subtracting out the distance from the 3DR position solution the position solutions can be differenced to display the accuracy and precision of the 3DR GPS kit.

**Zero Baseline Test**

The zero baseline test is a common test used for characterizing GPS receivers. It allows the researcher to isolate the errors in the receiver algorithms from the multitude of other errors affecting GPS measurements. Several configurations of zero baseline tests were conducted for this research. A zero baseline test with the Piksi units and a reference receiver gave insight into how the Piksi receiver performs relative to a higher cost component. The configuration for the zero-baseline test is shown in Figure 3-1.

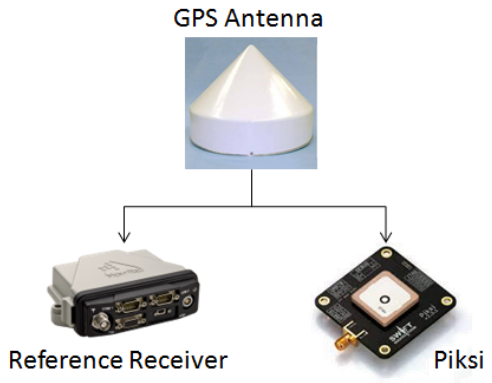


Figure 3-1: Zero baseline test schematic

Two types of data were collected during the zero-baseline test: position solutions and raw measurements. The position solutions are the computed latitude, longitude and height that are output from each of the receivers. The raw measurements consist of pseudorange in meters, carrier phase in cycles and carrier to noise ratio ($C/N_0$) measured in db-Hz. When compared to each other, the raw measurements give insight into how the algorithms running on the Piksi receivers function and potential limitations of the system.

**Zero Baseline RTK Test**

An additional zero baseline test was conducted to test the Piksi' s RTK algorithm. The test configuration is shown in Figure 3-2.

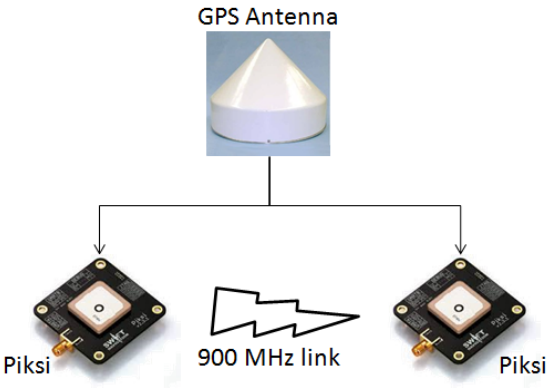


Figure 3-2: Zero baseline RTK test schematic

Similar to the test with the reference receiver, the test with the two Piksi receivers captured two types of data: position and raw measurements. The difference for this test was that for the position solution, the measurements were the relative position of one Piksi relative to the other. This measurement, referred to as the baseline, is measured in a local-level, north-east-down, coordinate frame. Since both receivers are getting measurements from the same antenna, the baseline measurements should be near zero. Any deviation from zero is the error in the RTK position solution

The raw measurements were also analyzed to give further insight regarding the differential calculation that is being computed. Since both receivers are getting measurements from the same satellites, the pseudorange and carrier phase measurements should be very close. Further, since the system is designed for utilizing the carrier phase measurements, it was hypothesized that the carrier phase measurements would be very close to each other since the baseline length is zero. Further RTK GPS algorithm testing was also conducted in a non-zero baseline configuration.

The communication modems within the Piksi RTK system, represented by the 900 MHz link in Figure 3-2, were upgraded from the lower power 100 mW 3DR modem included with the Piksi kit to 1W RFD 900+ modems. This upgrade was made to increase the effective range between the base and mobile receivers if the system is integrated onto a UAS. Additionally, the RFD 900+ is capable of one-to-many communications versus the standard one-to-one communication. The one-to-many communications architecture would allow for a simpler communication architecture if more than two Piksi receivers are implemented for a particular application such as formation flying. The consequence of using the RFD 900+ was that a non-

standard connector needed to be implemented. The pinout for the connector is shown in Figure 3-3.

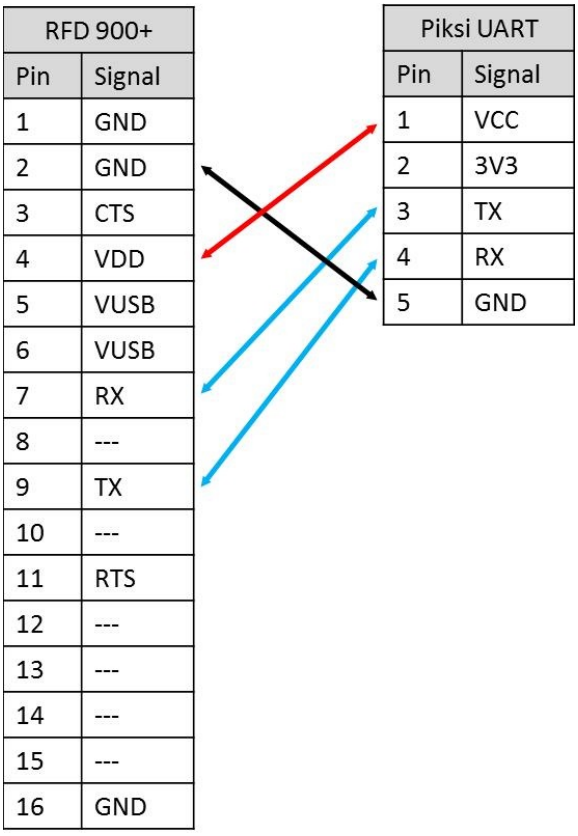

| RFD 900+ | |
|---|---|
| Pin | Signal |
| 1 | GND |
| 2 | GND |
| 3 | CTS |
| 4 | VDD |
| 5 | VUSB |
| 6 | VUSB |
| 7 | RX |
| 8 | --- |
| 9 | TX |
| 10 | --- |
| 11 | RTS |
| 12 | --- |
| 13 | --- |
| 14 | --- |
| 15 | --- |
| 16 | GND |

| Piksi UART | |
|---|---|
| Pin | Signal |
| 1 | VCC |
| 2 | 3V3 |
| 3 | TX |
| 4 | RX |
| 5 | GND |

Figure 3-3: RFD 900+ to Piksi connector pinout

**Real-Time Kinematic GPS Test**

To demonstrate the precision and accuracy of the Piksi RTK system in a field environment other than the zero-baseline tests, a series of tests were conducted using an existing AFIT RTK system as a truth source. The AFIT RTK system, which has been characterized to have accuracy within several millimeters, utilizes a NovAtel triple-frequency receiver as the base station to determine the error corrections communicating via an Ethernet bridge to a NovAtel dual-frequency receiver mounted on a golf cart as the mobile station.

The testing of the Piksi system was accomplished using several setups to show how the position solution changes for different applications. Table 3-1 shows the configuration of the accomplished tests.

Table 3-1: Test Configurations

| Test # | Base Antenna | Mobile Antenna | Stationary |
|---|---|---|---|
| 1 | Ashtech Choke-ring | NovAtel Pinwheel | Yes |
| 2 | Ashtech Choke-ring | Piksi Ext Antenna | Yes |
| 3 | Piksi Ext Antenna | NovAtel Pinwheel | Yes |
| 4 | Piksi Ext Antenna | Piksi Ext Antenna | Yes |
| 5 | Ashtech Choke-ring | NovAtel Pinwheel | No |
| 6 | Ashtech Choke-ring | Piksi Ext Antenna | No |
| 7 | Piksi Ext Antenna | NovAtel Pinwheel | No |
| 8 | Piksi Ext Antenna | Piksi Ext Antenna | No |

As shown in the table, the variables tested were the different antennas used by each receiver as well as whether or not the mobile antenna was fixed or moving. The Ashtech Choke-ring antenna referred to in Table 3-1 is a stationary dual frequency antenna located on the roof of AFIT at a surveyed absolute position. The Choke-ring integrated into the antenna provide multipath rejection. By knowing the absolute location of the base antenna, it is then possible to determine the absolute error of the relative position vector that is output by the Piksi. For the tests in which the base Piksi is connected to the external GPS antenna supplied with the Piksi kit, the absolute position was computed from the average position that was output from the Piksi receiver over a period of an hour. It was possible to obtain a higher fidelity absolute position of the base Piksi by surveying a location and then placing the Piksi antenna at that location; however, this test simulates a field user that is solely relying on the Piksi receivers for measurements. The results found in Chapter 4 will show that using the averaged position output from the Piksi receiver introduces a constant bias in the observed error in the absolute position of the mobile Piksi receiver.

The NovAtel Pinwheel antenna is a dual frequency antenna that, similar to the Ashtech Choke-ring antenna is designed to reject multipath errors. An antenna splitter was used when utilizing the NovAtel Pinwheel as the mobile antenna. This allowed the same measurements to be sent to both the Piksi receiver and the NovAtel truth source. The antenna splitter was not used for tests utilizing the Piksi external antenna since the antenna is only a single frequency antenna and therefore could not be used with the existing AFIT RTK system. In order to calculate the statistics associated with the Piksi RTK system while utilizing the Piksi external antenna as the mobile antenna, the offset between the AFIT RTK system antenna and Piksi RTK system antenna was computed from the distance and heading between the two antennas.

In addition to the eight tests, all with a stationary base antenna, a single test was conducted to show the effectiveness of the Piksi RTK system to perform while both the base and mobile receiver are in motion. For this test, the configuration shown in Figure 3-2 was mounted to a mobile platform along with the AFIT RTK system. The AFIT RTK system was utilized to get high-precision position measurements to show the movement of the platform since the baseline position solutions output by the Piksi system will not show movement. The positions of the AFIT RTK system's antenna were computed in a local level coordinate frame centered at the base antenna's known location.

Error Calculation

The calculation of the relative position error was altered given the different preconditions for the tests. This was done to show how accurate and precise the Piksi RTK system is for several scenarios. For Test #1 and #5 the position solution of the AFIT RTK system, represented in the global coordinate frame, were converted to a local level coordinate frame centered at the known, surveyed, location of the base antenna. The computed error in the Piksi RTK system

was then the difference between the two solutions. Test #2 required the offset between the mobile Piksi antenna and the NovAtel Pinwheel to be computed in the local level coordinate frame referenced by the Piksi receiver. A schematic showing the offset calculation is shown in Figure 3-4.

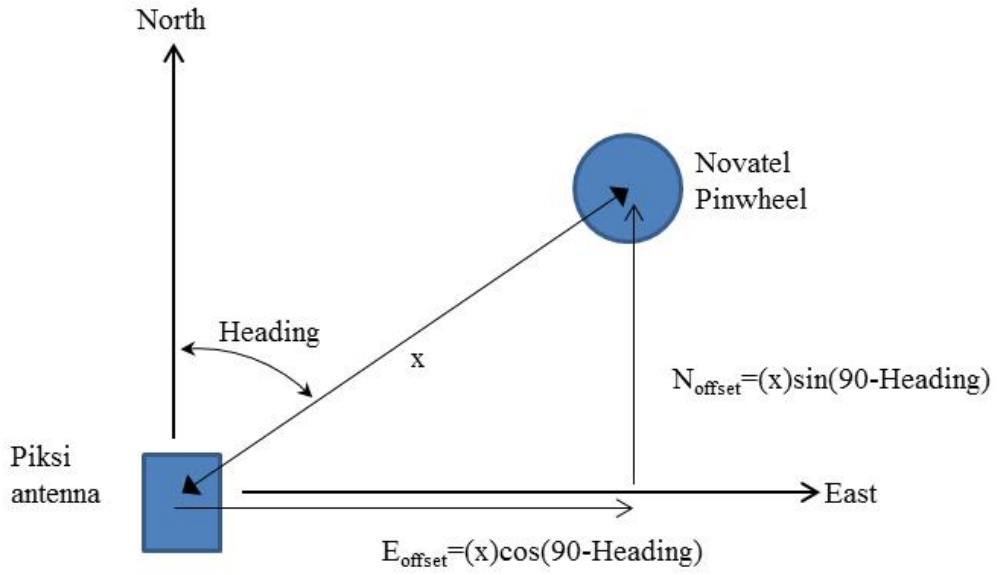


Figure 3-4: Offset calculation schematic

This offset calculation was completed for each of the stationary tests that used the Piksi external antenna as the mobile antenna. To compare the outputs of the Piksi RTK system to the AFIT RTK system, the computed offsets were added to the outputs of the Piksi RTK system and then subtracted from the results from the AFIT RTK system. Since a data-logging compass was not available this offset calculation could not be done for Test #6 and #8. Because of this constraint the data from these tests will only show whether or not the system could maintain the RTK solution using the Piksi external antenna on a mobile platform. If one were to be integrated into the test setup, then it would then become necessary to calculate the offsets for each data sample.

**Integration Test**

Integrating the Piksi system onto a small-UAS was not fully accomplished under this work. However, a series of tests were conducted to show the usability and applicability of the system. The test consisted of vibration testing as well as simulated flight testing.

The vibration testing was conducted in order to determine if the crystal oscillator within the Piksi circuit board would be affected by low-amplitude, high-frequency, external vibrations caused by the motor onboard the UAS. To show the effects of the vibration on the system, the zero-baseline RTK test setup was implemented with one of the receivers affixed to a small shaker table. The amplitude of the shaker table was set at 2.5 mm while the frequency was varied from 40 to 200 Hz in 10 Hz increments. Both the amplitudes and frequencies were chosen to be at the high end of the range of vibrations that the Piksi receiver would encounter on a UAS. The amplitude to use was determined from research conducted by Tint et al. characterizing the vibration of a lawn mower engine, which is comparable to engines utilized by small gas-powered UASs [27]. The range in frequency was taken from literature on the operating revolutions per minute of small gas engines employed by UASs. The vibration testing was done with the Piksi mounted in 3 orthogonal planes to show how the orientation of the Piksi receiver within the UAS would affect the system. Any deviation from the baseline length of zero, greater than what is realized during the zero-baseline RTK test, will show effects of the vibration on the system.

The simulated flight testing was conducted to show how the Piksi system could be implemented onto a rolling aircraft. Because RTK systems operate by tracking carrier phase cycles, it is imperative that the algorithms be robust enough to maintain the RTK solution while satellites are coming in and out of view of the antenna. The robustness of the algorithms is

especially important for UASs where the metal ground plane attached to the GPS antenna will block the GPS signal when the aircraft pitches and rolls at high angles. For the test, a simulated UAS consisting of a Piksi receiver connected to the Piksi external GPS antenna, a Pixhawk autopilot and a 3DR GPS unit were attached to a yardstick. The simulated UAS could then be pitched and rolled to demonstrate how the Piksi receiver handles satellites coming in and out of view as the aircraft is rolled. Additionally, the test demonstrated how the Pixhawk autopilot uses the two GPS solutions for the position solution of the UAS. A schematic of the test setup is shown in Figure 3-5.

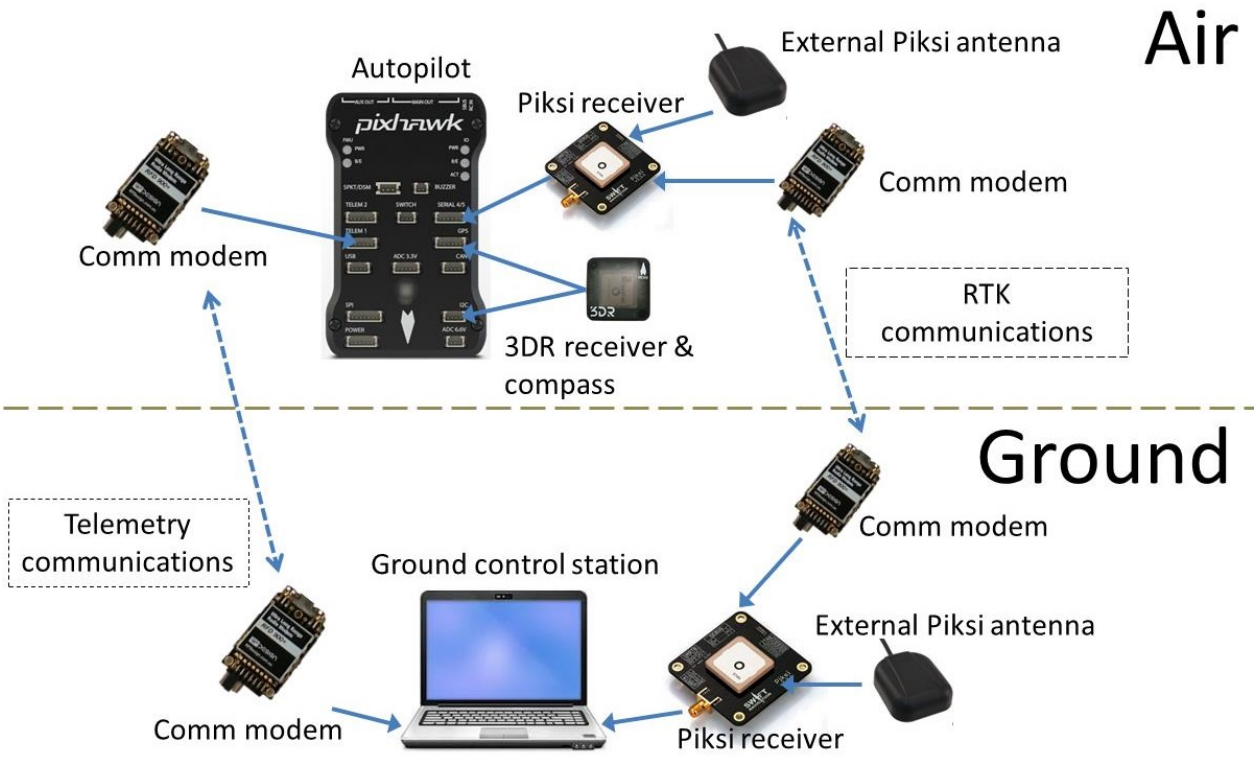


Figure 3-5: Integration test setup

**Summary**

This chapter laid out the methodology utilized to garner the key data for this thesis. First the method used to calculate the accuracy and precision was discussed. Then the method used to

demonstrate the accuracy and precision of the hobbyist standard 3DR GPS kit was detailed. After which, the zero-baseline test was laid out to measure the accuracy and precision of the Piksi receivers in a standalone configuration as well as the RTK configuration. Then the method used to characterize the accuracy of the RTK GPS solutions for several antenna configurations was detailed. Finally, the high-level integration test procedures were discussed. The next chapter will discuss the results of the aforementioned tests.

# 4. RESULTS & DISCUSSION

This chapter discusses the results from the tests conducted in line with the methods laid out within Chapter 3.

## 3DR GPS Kit Characterization

The 3DR GPS kit was tested to show the improvement in both accuracy, represented by average error, and precision, represented by the standard deviation, by utilizing a RTK GPS system. As discussed in Chapter 3 the test was conducted by utilizing a short baseline test. The truth position was obtained by taking the time averaged absolute position output by the AFIT RTK system from 60 minutes of data. This absolute truth position was the origin of the local level coordinate frame for the calculation of the statistics related to the 3DR GPS kit. The East-North position solutions from the 3DR GPS kit, represented in a local-level coordinate frame, are displayed in Figure 4-1.

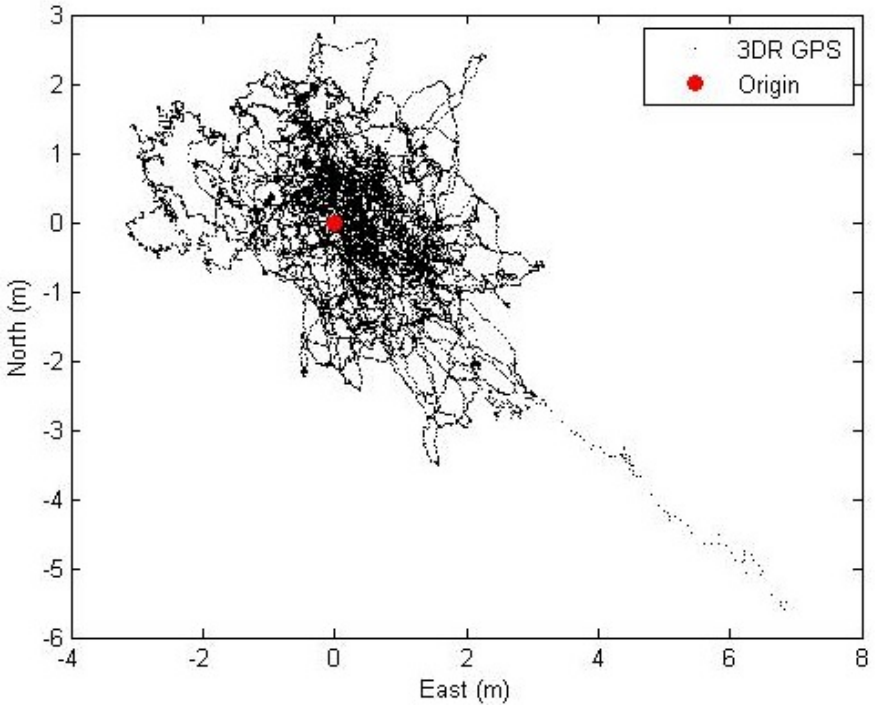


Figure 4-1: 3DR GPS kit North-East position solutions in local-level coordinate frame

The data represented in the bottom right-hand side of the plot are position solutions immediately after powering on the receiver. Removing those data points shows an elliptical spread of data points consistent with a Gaussian distribution.

The limiting factor for low-cost GPS receivers is the receiver clock error. This limitation is shown in the error of the height measurements. Figure 4-2 depicts the height position solutions in the local-level East-Up coordinate frame.

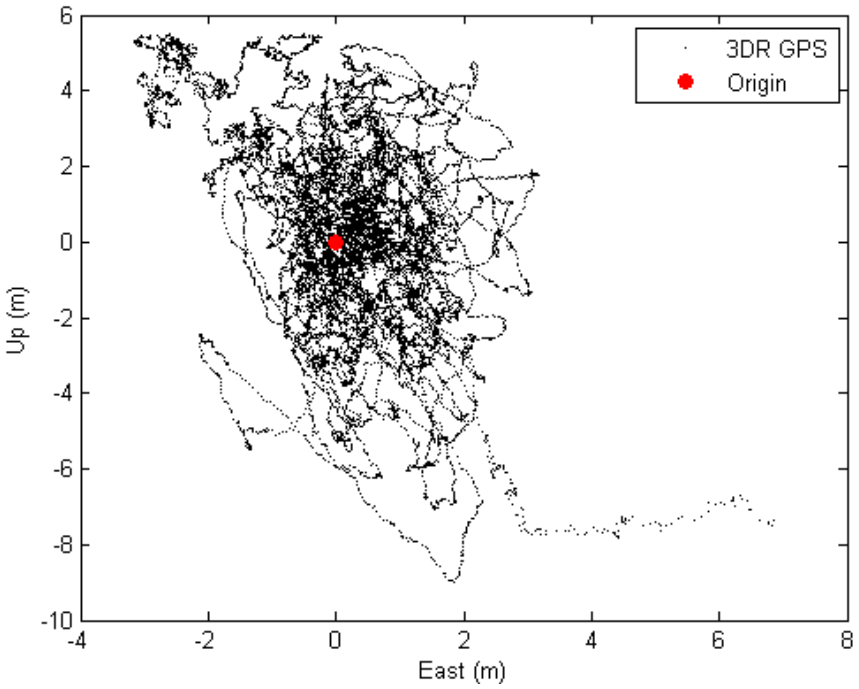


Figure 4-2: 3DR GPS kit East-Up position solutions in local-level coordinate frame

Similar to Figure 4-1, the data points on the right-hand side of the plot are from the initial startup of the receiver. Figure 4-2 shows that the distribution of data points from the 3DR GPS receiver kit also follow a Gaussian distribution in the East-Up frame.

To obtain a better understanding of the magnitude of the error in each direction the components of the position solutions are plotted individually. The error in each direction over the sixty minute test time is displayed in Figure 4-3.

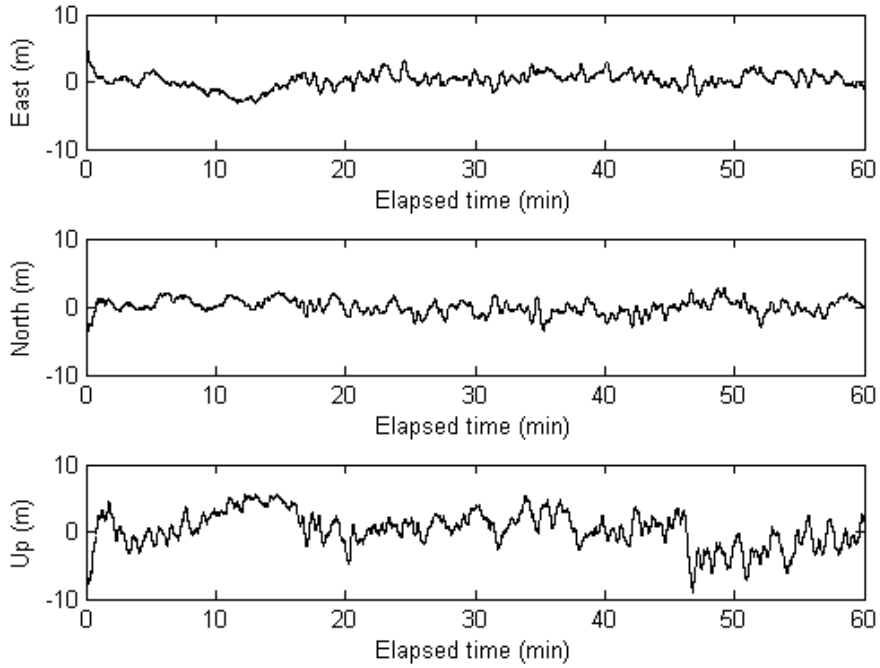


Figure 4-3: 3DR GPS kit position solution error

As shown in the figure above, the position error is about equal in the North and East components of the position solution. As expected, the Up component displays a standard deviation that is above twice the magnitude as the East and North components. Table 4-1 further clarifies the average and standard deviation of the error in each direction.

Table 4-1: 3DR Error Statistics

| | **East** | **North** | **Up** |
|---|---|---|---|
| Mean Error (m) | 0.25 | 0.01 | 0.26 |
| Standard Deviation (m) | 1.15 | 1.06 | 3.97 |

Using the equations found in Chapter 3, the accuracy and precision measures are found in Table 4-2.

Table 4-2: 3DR GPS kit accuracy and precision measures

| **Measure** | **Value (m)** |
|---|---|
| DRMS | 1.58 |
| MRSE | 3.08 |
| $\sigma_{2D}$ | 1.56 |
| $\sigma_{3D}$ | 4.26 |

In addition to characterizing the 3DR GPS receiver kit as a standalone receiver, work was also accomplished to evaluate the efficacy of utilizing the 3DR kit in a differential setup. Since the kit is not capable of outputting the raw measurements, such as carrier phase and pseudorange, the differential setup utilizing the 3DR GPS kit would need to function using only the position solutions. For this setup one 3DR GPS kit would be designated as the base receiver while the other is designated the mobile receiver. The base receiver would be stationary at a known, surveyed, location while the mobile receiver is free to move. A processor would then use the calculated error in the base receiver's position solution, calculated by taking the difference in the known location versus the output solution by the 3DR GPS kit, to correct the position solution of the mobile receiver. This application of the offset could be done in real-time, much like RTK systems work, to allow for higher accuracy positioning of the mobile receiver.

To test this architecture, a short baseline test was conducted using two 3DR GPS receiver kits, designated GPS1 and GPS2. GPS1 was designated as the base receiver for this test. After subtracting out the short baseline between the two receivers, the position solutions should, if the differential system is to be effective, be very close to each other. Figure 4-4, plotted in a local-level coordinate frame with the first data point from GPS1 as the origin, shows that this is not the case.

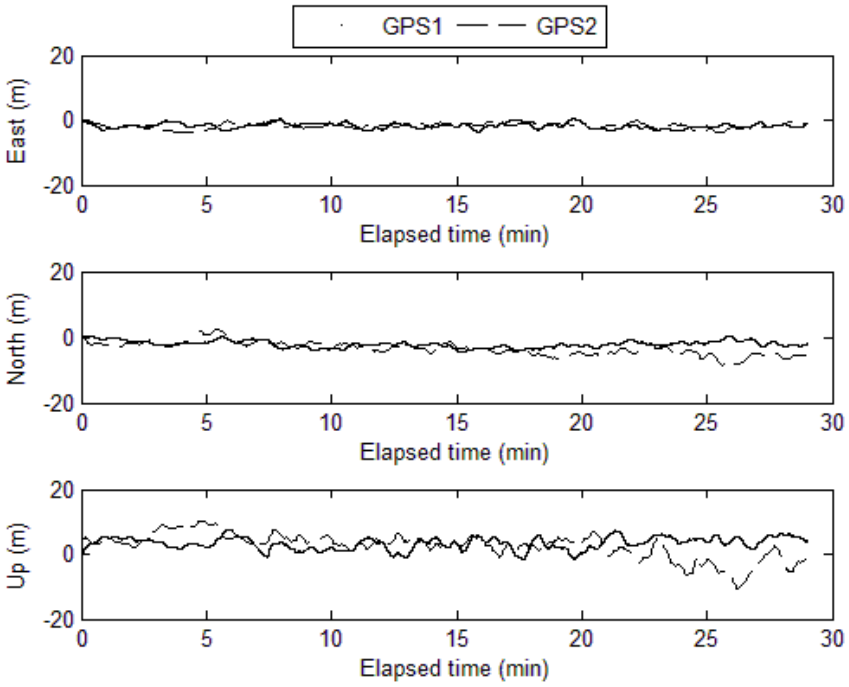


Figure 4-4: Short baseline test results

While the relative error between the two receivers is relatively small, it is not a constant offset that could be applied to the mobile receiver resulting in higher accuracy. To further show the non-constant offset, Figure 4-5 shows the output of GPS2 subtracted from GPS1.

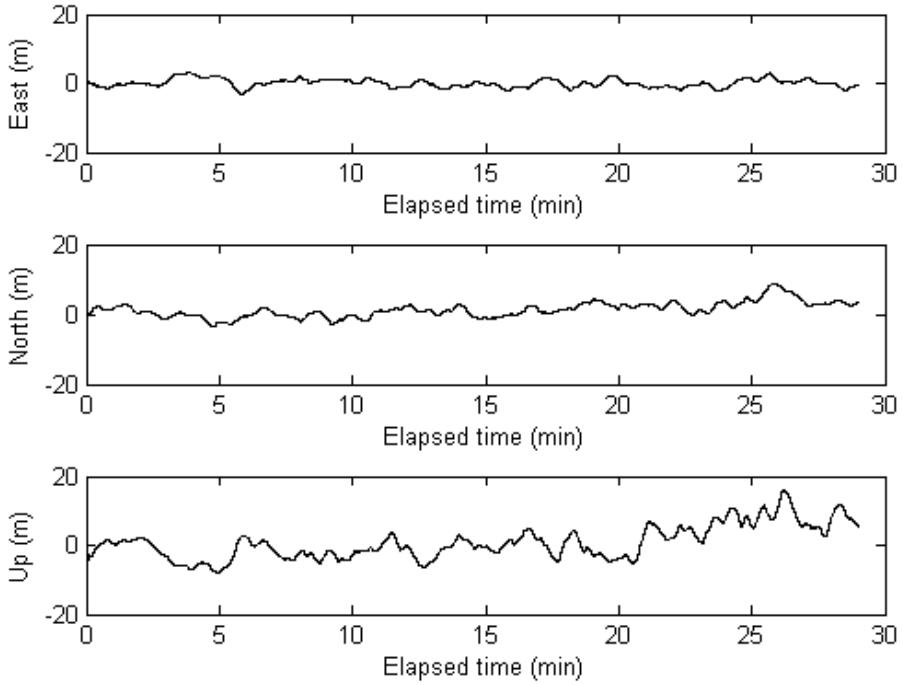


Figure 4-5: 3DR Differential Output Error

Tabulated statistics derived from Figure 4-5 are found in Table 4-3.

Table 4-3: 3DR Differential Error Statistics

| | East | North | Up |
|---|---|---|---|
| Mean Error (m) | 0.036 | 1.312 | 0.770 |
| Standard Deviation (m) | 1.199 | 2.177 | 4.821 |

Comparing Table 4-1 and Table 4-3 shows that utilizing the 3DR GPS kits in a differential GPS system does not offer any improvements to the accuracy or precision of the position solution.

**Zero Baseline Test**

For this research two sets of zero baseline tests were conducted; one to test the accuracy and precision of the Piksi receiver as a standalone receiver, the other to test the accuracy and precision of the Piksi RTK system. As noted in Chapter 3, testing of the Piksi as a standalone receiver was done in reference to a higher cost GPS receiver. The reference receiver utilized by this research was a NovAtel DL-V3. To obtain the accuracy of the Piksi, an antenna with a

known, surveyed location was utilized. The position solution results are plotted in a local level coordinate frame centered at the known location of the GPS antenna. Components of the position solution of both the Piksi and reference receiver are shown in Figure 4-6.

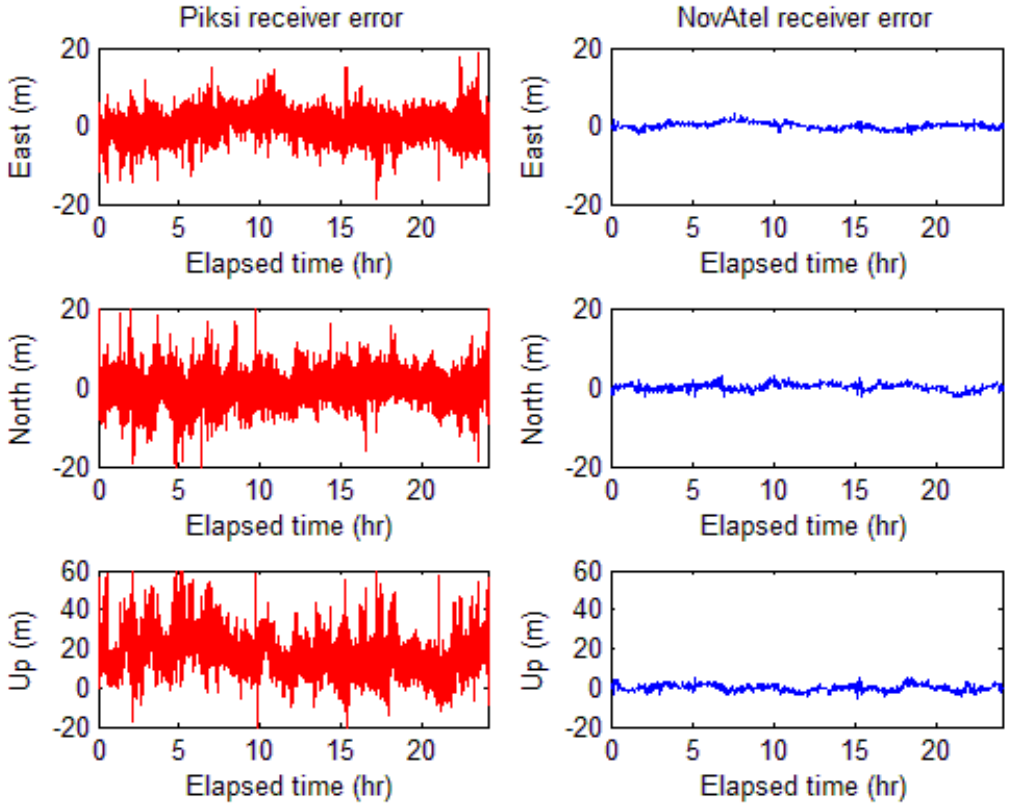


Figure 4-6: Zero baseline position solution error

From the plots, it is evident that the Piksi receiver, operating as a standalone GPS receiver, is not as precise as the reference receiver. Further information regarding the accuracy and precision of the Piksi can be found in the tabulated error statistics within Table 4-4 and Table 4-5.

Table 4-4: Piksi receiver error

| | East | North | Up |
|---|---|---|---|
| Mean Error (m) | -0.081 | 0.108 | 18.894 |
| Standard Deviation (m) | 3.044 | 3.697 | 9.858 |

Table 4-5: Reference receiver error

| | East | North | Up |
|---|---|---|---|
| Mean Error (m) | -0.020 | 0.076 | 0.026 |
| Standard Deviation (m) | 0.747 | 0.829 | 1.518 |

The results show that while the Piksi is roughly as accurate as the reference receiver in the East and North directions, a potential limitation of the receiver is realized in the Up direction. This is likely due to the implementation of a smaller, lower-cost oscillator on the Piksi receiver. Additionally, when comparing the error statistics of the 3DR GPS receiver kit to the results of the Piksi, it is clear that the Piksi receiver is not a good alternative to the 3DR GPS kit.

Collecting and evaluating the raw data from the Piksi gave some insight into why the receiver did not perform very well relative to the reference receiver. Pseudorange, carrier phase and carrier to noise ratio measurements were collected from both the Piksi and reference receiver. Before analyzing the raw measurement, the sensitivity of the Piksi receiver to lock onto the GPS satellite's signal was evaluated by plotting the GPS satellites in view for each receiver. A plot showing the visible GPS satellites, designated by the PRN, throughout the data collection period is shown in Figure 4-7.

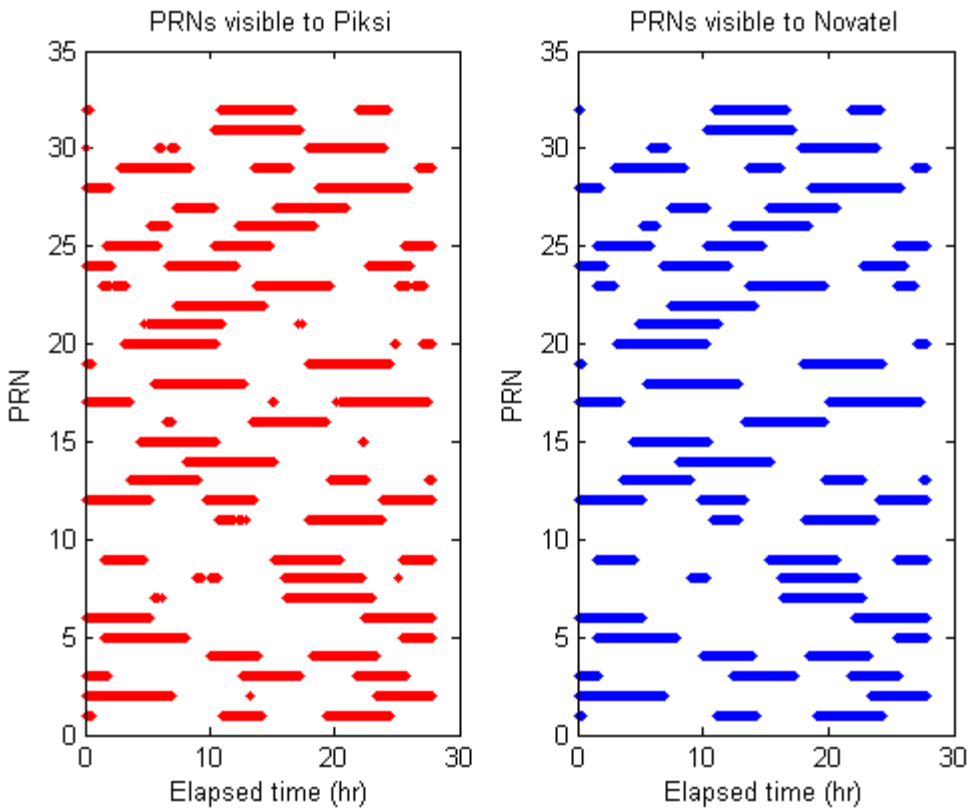


Figure 4-7: Visible PRNs

Figure 4-7 shows that on a macro-scale, the Piksi receiver was locked onto the same GPS satellites as the NovAtel receiver. A more careful examination of the plot, however, shows some discrepancies. A clearer understanding of the difference between the two receivers is shown by slightly offsetting the Piksi PRN number and plotting the data on the same axis. This plot is shown in Figure 4-8.

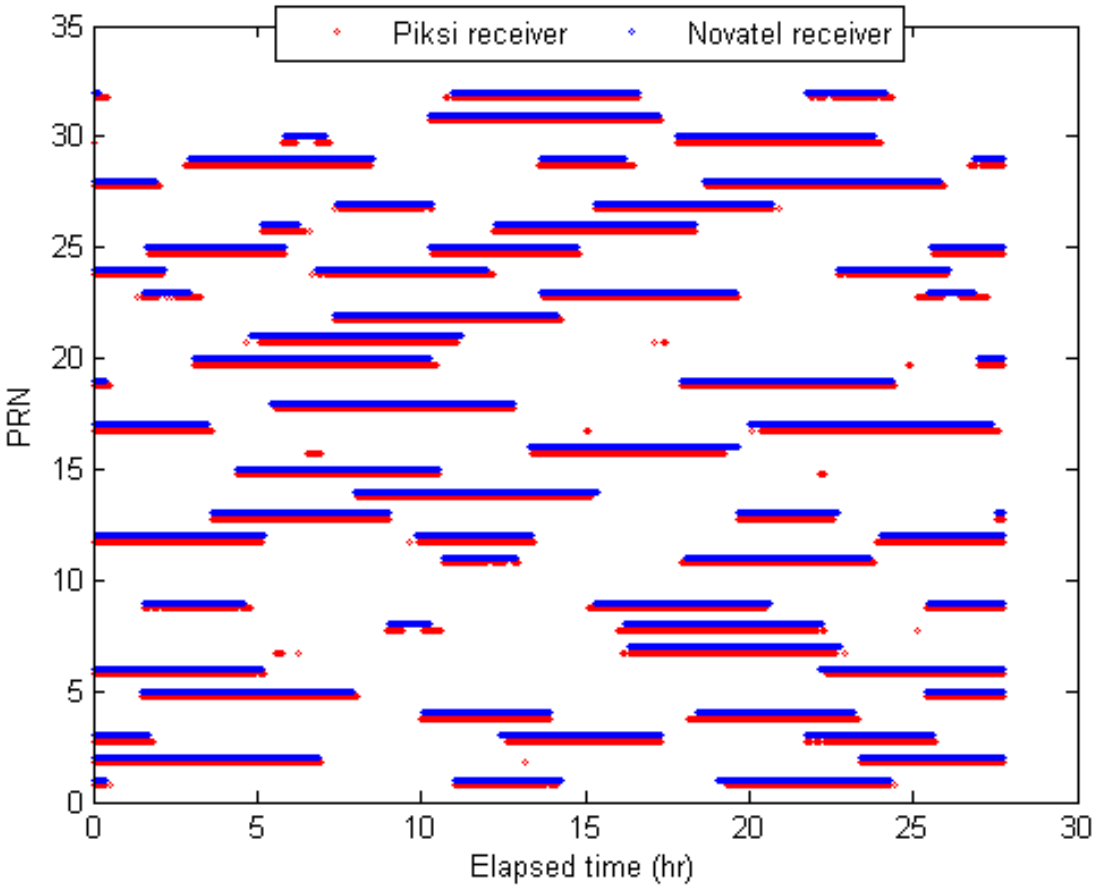


Figure 4-8: Visible PRNs Comparison

Prior to analyzing the data, it was assumed that the higher-end components present in the NovAtel receiver would allow for the NovAtel to lock onto PRNs and maintain lock for a longer period of time. After examining the figure above, it is clear that the Piksi receiver was able to lock onto the PRNs as quickly and in some cases, quicker, than the NovAtel receiver. There are a couple other anomalies present in Figure 4-8. One anomaly present in Figure 4-8 is the Piksi receiver losing lock on a PRN about half way through the time that the same PRN is visible to the NovAtel receiver. This phenomenon is observed when taking a closer look at the results from PRN 23. The first time during the data collection that PRN 23 is visible the Piksi receiver locks onto the PRN prior to the NovAtel, and then the Piksi loses lock on the PRN while the NovAtel receiver maintains lock. The relatively short duration that the PRN is visible, roughly

one hour, means that the satellite was likely very low in the sky. The plot in Figure 4-9 shows that during the time that the Piksi receiver loses lock, the satellite is less than 10 degrees above the horizon.

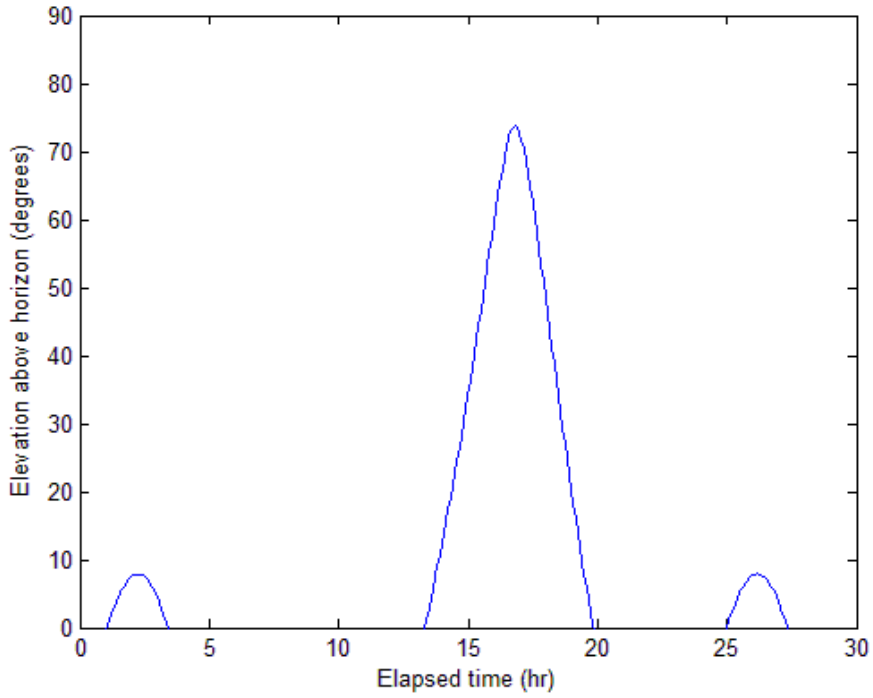


Figure 4-9: PRN 23 elevation versus time

The loss of lock on the PRN by the Piksi receiver, gave an early indication that the Piksi receiver may not have very good noise mitigation capabilities that cause the receiver to lose lock prematurely.

One other anomaly noted in Figure 4-8 is the Piksi incorrectly locking onto a PRN for a short period of time. One example of this is found by looking at the results for PRN 16. For about a half hour, roughly six hours into the data collection, the Piksi receiver incorrectly locks onto PRN 16. This anomaly cannot be as easily explained as the first, but is likely due to a lack of noise mitigation within the Piksi receiver. Examining the carrier to noise ratio of the receiver will show how well each of the receivers handle noisy signals.

Evaluating the carrier to noise ratio showed how well the noise filters operating on board the Piksi receiver operate relative to the NovAtel receivers. Figure 4-10 shows the carrier to noise ($C/N_0$) plotted against elevation for PRN 5, one satellite that passes nearly overhead during data collection.

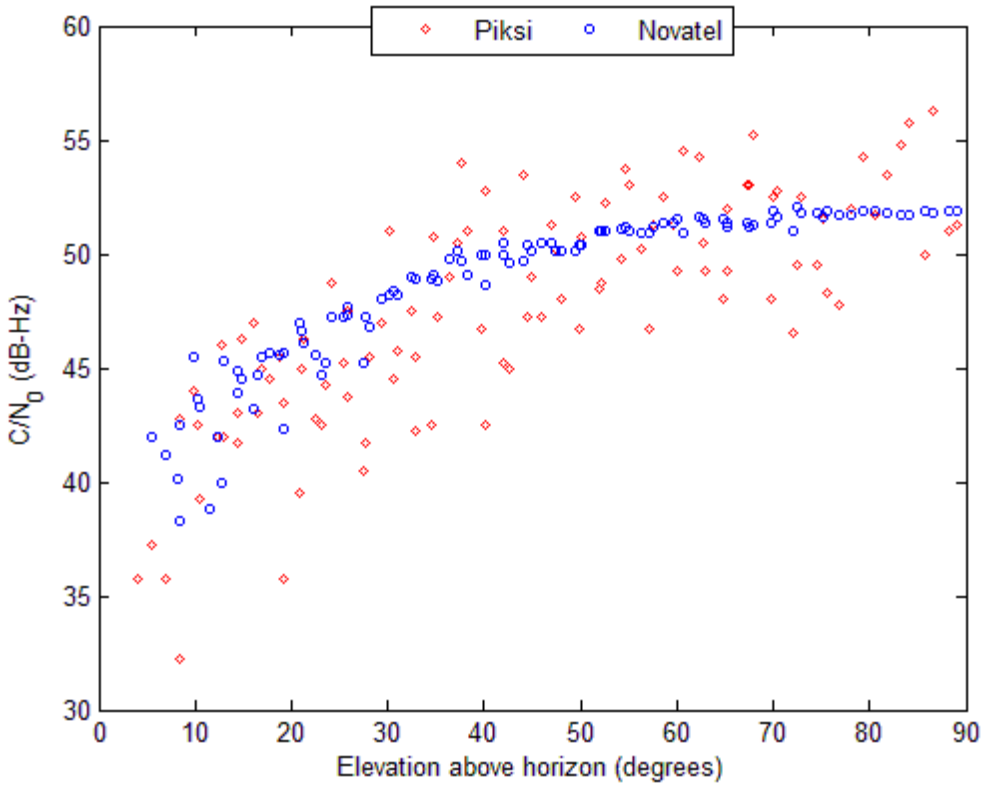


Figure 4-10: PRN 5 C/N0 versus elevation

The overall trend of Figure 4-10 is due to the fact that at lower elevations, the GPS signal is required to travel through more of the Earth's atmosphere causing a noisier signal. The plot shows that, even at high elevation angles when C/N0 is at its maximum, the variance of the C/N0 of the Piksi receiver is very high compared to the NovAtel receiver. This trend is not surprising, however, after examining Figure 4-8, and explains why the Piksi receiver could lose lock on a PRN even while the satellite has a higher elevation.

The next raw measurement investigated was the pseudorange measurements derived from the C/A code. To add some additional insight regarding the error in the pseudorange measurement, the true range was also calculated based from precise ephemeris information that is calculated and maintained by the National Geospatial-Intelligence Agency [17]. As noted in Chapter 2, the difference between the true range and the pseudorange is the measurement errors.

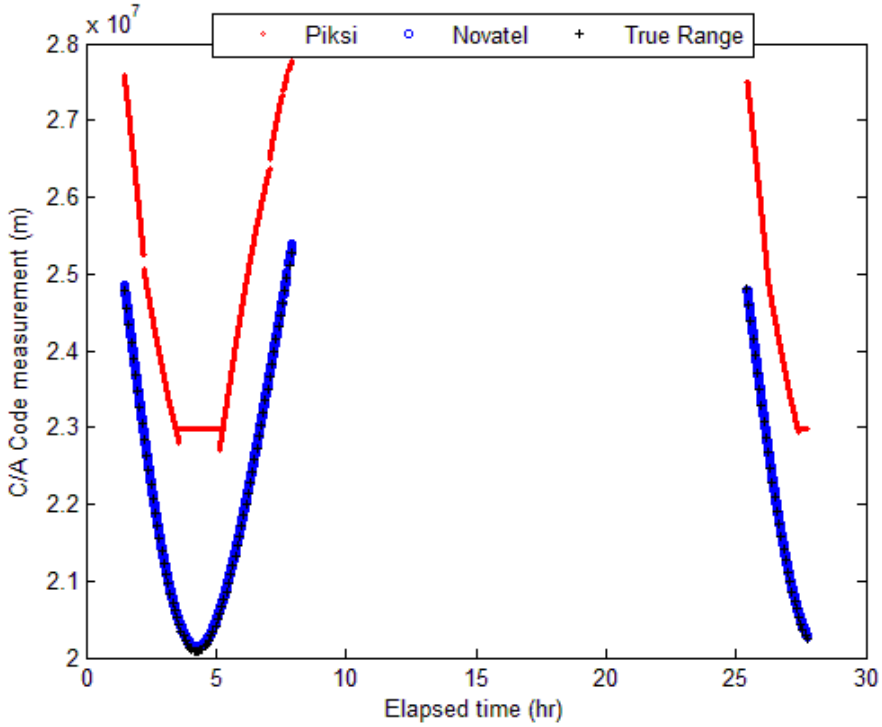


Figure 4-11: PRN 5 Pseudorange measurements

The results in Figure 4-11 show that while the NovAtel closely follows the true range, the Piksi receiver is off by about $3x10^6$ meters throughout the orbit. One additional note to make about the pseudorange measurement of the Piksi receiver is the flattening of the parabola shape at the closest ranges. This helps to explain how the Piksi is calculating the pseudorange from each satellite. At each instant, the Piksi receiver selects PRN pseudorange to keep constant. It then uses that time differential as a baseline to compare to other PRN signals. The reference PRN at each time instant is shown in Figure 4-12.

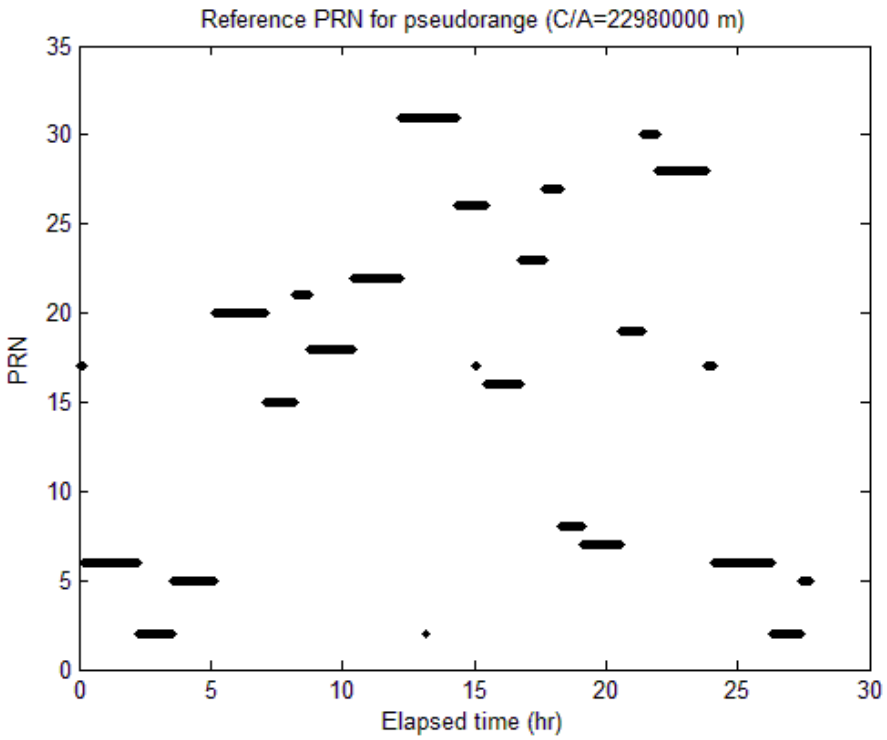


Figure 4-12: Reference PRN

This method of calculating the pseudorange likely requires less processing power that can be allocated to more computationally intensive tasks. It is not certain why the Piksi receiver calculates the pseudorange this way or how exactly the algorithms work because the software that does this calculation is not open source [22].

The carrier phase measurements were also not what they were expected to be. Figure 4-13 shows the measurement taken from the Piksi and NovAtel receivers. The truth source was calculated by dividing the true range by the L1 wavelength, 19 centimeters.

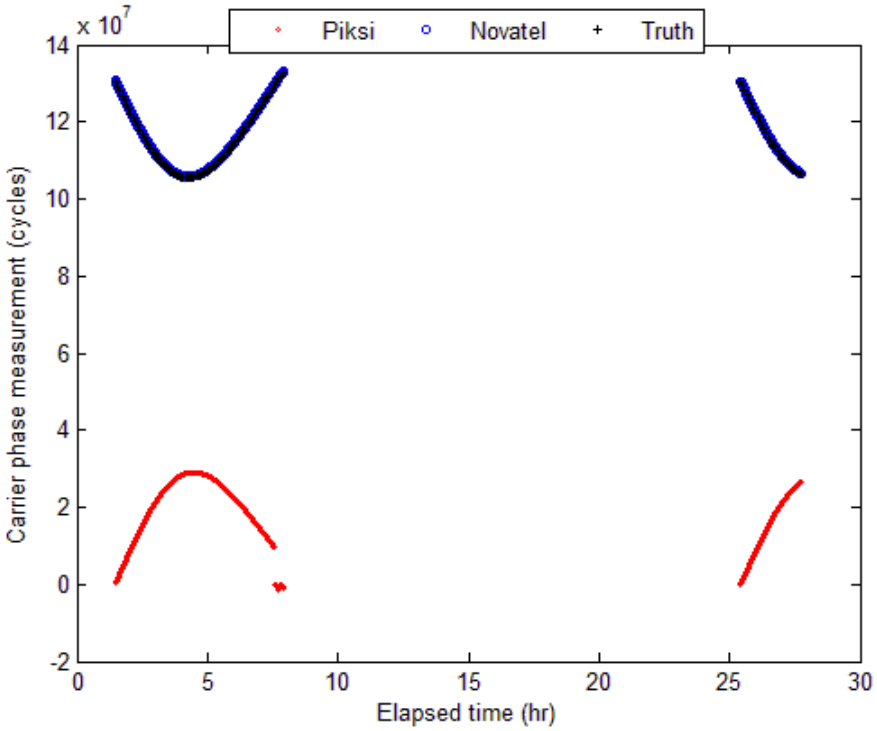


Figure 4-13: PRN 5 Carrier phase measurement

Similar to the pseudorange measurements, the NovAtel carrier phase measurements match the truth source very well. The Piksi's carrier phase measurements are not only off by a large offset, but are also inverted relative to the NovAtel and truth source. It is difficult to hypothesize what is causing this trend without having the source code, but it is likely a tradeoff made to decrease the required processing resources. Additionally, coupled with the pseudorange measurements, the carrier phase measurements are not able to be integrated with the open-source RTKlib that was utilized by Pilz et al. and Stempfhuber. This limits users from buying lower cost receivers and applying the Swift Navigation developed RTK algorithms to achieve the high accuracy position solutions.

The raw measurements taken from the Piksi receiver help to explain why the receiver's position solutions are much less precise than the NovAtel and 3DR receivers. While the data sample size is not very large, the results of the zero baseline test show that the Piksi receiver is

not a good alternate to the 3DR GPS receiver kit as a standalone receiver. The next zero baseline test will determine the accuracy and precision of the Piksi RTK system as it was intended to be implemented.

**Zero Baseline RTK Test**

Similar to the zero baseline test with the NovAtel reference receiver, the zero baseline RTK testing captured two types of data: position solutions and raw measurements. For this test the position solutions are output from the Piksi in a relative local level frame instead of the absolute frame that the position solutions were output for the first test. Since both the base and mobile receiver are connected to the same GPS antenna, each of the components of the position solution should be zero.

Data was collected for 12 hours at a one hertz collection rate to show robustness of the RTK algorithms as satellites are coming in and out of view. Throughout the 12 hour data collection, all satellites were observed. The results of the zero baseline RTK test are found in Figure 4-14.

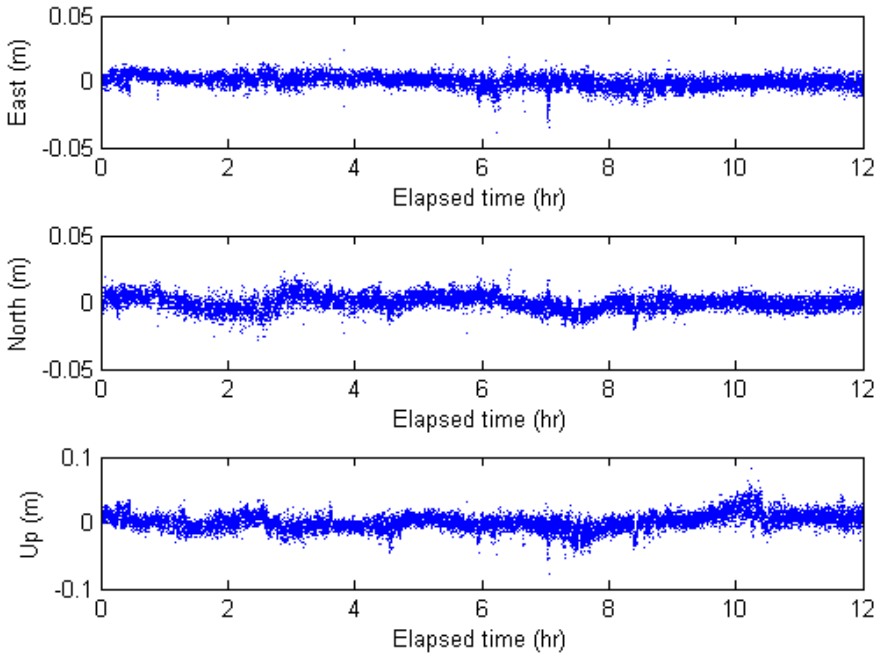


Figure 4-14: Zero baseline RTK results

The plotted results show that the measurements output by the RTK algorithms performed very well over the span of the test. The tabulated Gaussian error statistics, found in Table 4-6, along with the accuracy and precision statistics described in Chapter 3, found in Table 4-7, show that the Piksi's RTK algorithm accuracy is well within the 10 centimeter accuracy publicized by Swift Navigation.

Table 4-6: Zero baseline RTK error (1 Hz solution output)

| | **East** | **North** | **Up** |
|---|---|---|---|
| Mean Error (m) | < 0.001 | < -0.001 | -0.003 |
| Standard Deviation (m) | 0.004 | 0.005 | 0.012 |

Table 4-7: Zero baseline RTK accuracy and precision measures

| **Measure** | **Value (m)** |
|---|---|
| DRMS | 0.007 |
| MRSE | 0.014 |
| $\sigma_{2D}$ | 0.006 |
| $\sigma_{3D}$ | 0.014 |

This millimeter-level accuracy is, however, realized using the best-case scenario for the RTK algorithms. The spatially correlated errors, such as ionosphere and troposphere error, are effectively cancelled out since the measurements are being taken at exactly the same spot. As the distance between the two antennas increases, the measurement error will increase.

Data was also collected at two and five hertz to determine how the accuracy and precision of the Piksi RTK solution changes as the solution frequency is increased. The error in the position solutions from the two and five hertz collection rates are found in Table 4-8 and Table 4-9, respectively.

Table 4-8: Zero baseline RTK error (2 Hz solution output)

| | **East** | **North** | **Up** |
|---|---|---|---|
| Mean Error (m) | -0.001 | < 0.001 | -0.002 |
| Standard Deviation (m) | 0.005 | 0.006 | 0.012 |

Table 4-9: Zero baseline RTK error (5 Hz solution output)

| | **East** | **North** | **Up** |
|---|---|---|---|
| Mean Error (m) | < 0.001 | < 0.001 | -0.001 |
| Standard Deviation (m) | 0.005 | 0.004 | 0.009 |

Comparing the results to the results from the one hertz data, the Piksi RTK solution accuracy and precision are not appreciably affected by the changing frequency.

The raw measurements were also analyzed for trends that would give insight into how the Piksi RTK algorithms work. The goal of this research was not to reverse engineer the RTK algorithms, but the raw measurements are shown for scientific rigor. It was assumed that since both receivers were receiving the same signals from the antenna; the raw measurements would be very similar. The C/A code measurement, carrier phase and carrier to noise ratio versus time

for both receivers taken from PRN 31, which was the satellite that reached the highest elevation throughout testing, is shown in Figure 4-15.

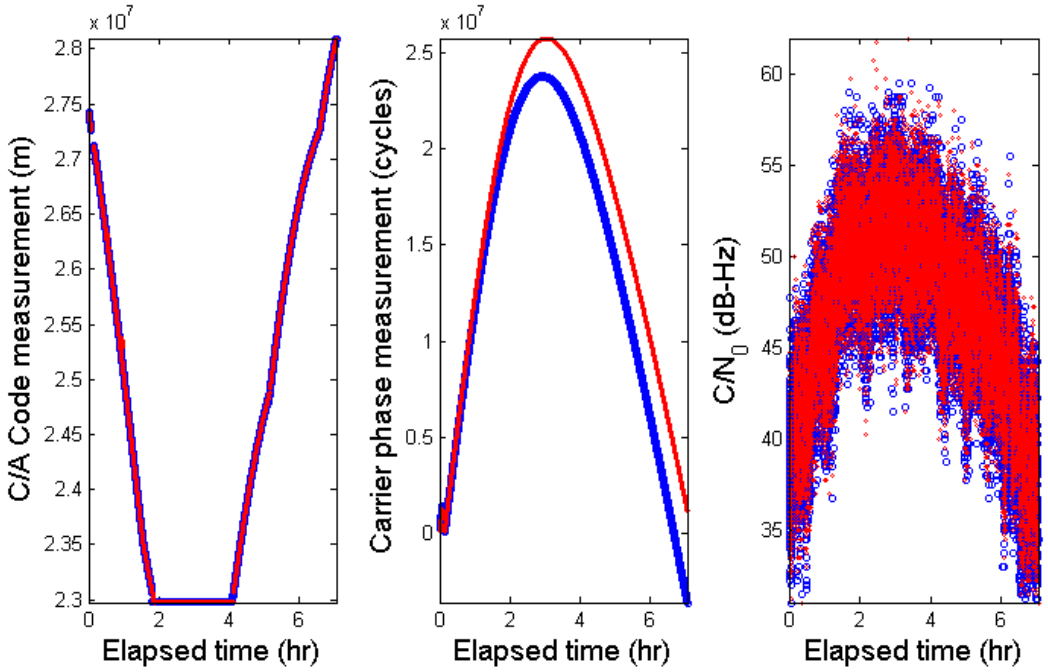


Figure 4-15: Zero baseline RTK raw measurements

The figure shows that the C/A code measurements are very close to each other throughout the time that PRN 31 was visible to both receivers. Examining the difference between the measurements shows that they match within 10 meters for the majority of the collection time. The difference between the carrier phase measurements reveals a straight line with a constant slope of about 190 cycles/second. This 190 cycles/second is the clock offset bias that is present when examining the data from each PRN visible during the test. In regard to the carrier to noise ratio, no apparent trend was found when taking the difference. The plot does show that neither receiver had a better $C/N_0$ than the other.

The zero baseline tests conducted within this research determined the accuracy and precision of the Piksi RTK system with minimal experiment-induced error. The following

sections will focus on the results of tests that will show how the system performs outside of a laboratory setting.

**RTK GPS Tests**

As discussed in Chapter 3, the performance of the Piksi RTK system was tested relative to a high-end RTK system possessed by AFIT, referred to as the AFIT RTK system. The configuration settings for each Piksi receiver were set at the manufacturer recommended settings. These settings can be found in Appendix A. The primary variable during the test was the antenna chosen to supply the receiver with raw measurements along with determining how the system performed while the mobile receiver was not stationary. Stationary and non-stationary tests were conducted so that errors induced by a moving platform could be easily discernible. The test configurations were specified in Table 3-1 and are shown below for the reader's convenience.

Table 3-1: Test Configurations

| Test # | Base Antenna | Mobile Antenna | Stationary |
|---|---|---|---|
| 1 | Ashtech Choke-ring | NovAtel Pinwheel | Yes |
| 2 | Ashtech Choke-ring | Piksi Ext Antenna | Yes |
| 3 | Piksi Ext Antenna | NovAtel Pinwheel | Yes |
| 4 | Piksi Ext Antenna | Piksi Ext Antenna | Yes |
| 5 | Ashtech Choke-ring | NovAtel Pinwheel | No |
| 6 | Ashtech Choke-ring | Piksi Ext Antenna | No |
| 7 | Piksi Ext Antenna | NovAtel Pinwheel | No |
| 8 | Piksi Ext Antenna | Piksi Ext Antenna | No |

The results from each of the tests are presented both in tabulated results and via a plot of the position solutions. Tests #6 and #8 do not have truth data associated with the tests; therefore statistics were not calculated for these tests. These tests will show the ability of the Piksi RTK system to operate with the antenna configuration.

The antenna configuration was identical for Test #1 and #5. These were also subjected to the least amount of test-induced error since the Piksi RTK system shared antennas with the AFIT RTK system via an antenna splitter. A schematic of the test setup for Test #1 is found in Figure 4-16. For Test #5, the antenna setup was the same as Test #1; however, the golf cart, which houses the mobile antenna, was not stationary throughout the test.

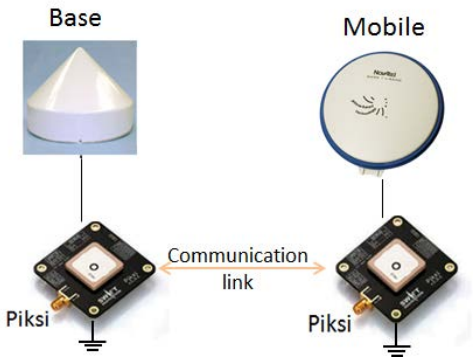


Figure 4-16: Test #1 setup [17] [20] [22]

To calculate the Piksi RTK solution error, a coordinate frame transformation was computed to change the AFIT RTK solutions in the absolute coordinate frame to the local level coordinate frame used by the Piksi RTK system. The transformed AFIT RTK solutions could then be directly compared to the Piksi RTK solutions. The components of the error from Test #1 are shown in Figure 4-17.

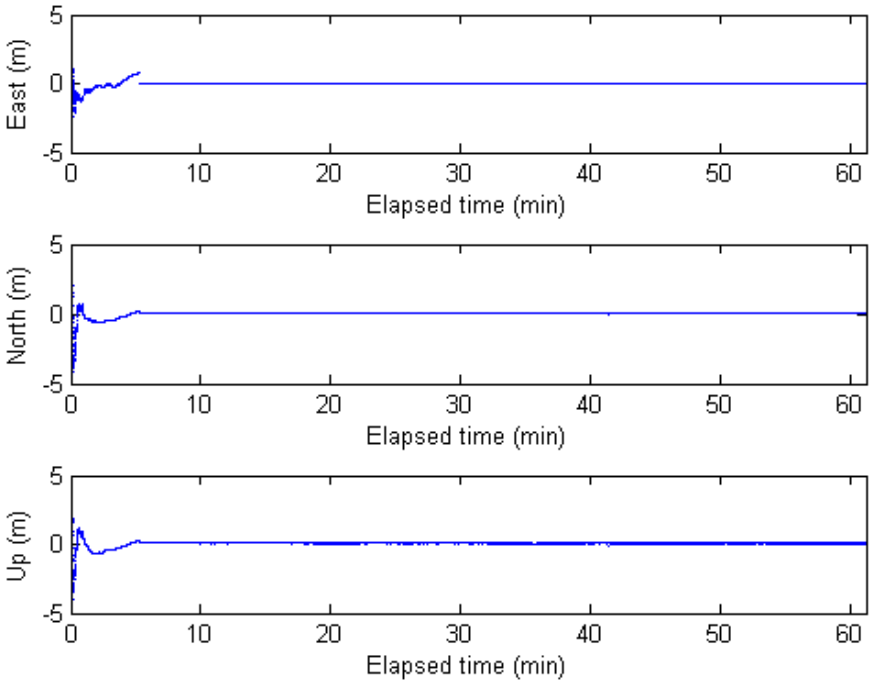


Figure 4-17: Test #1 position solution errors

As shown in the figure, the error in the Piksi solution is high for about the first five minutes. The Piksi RTK system, then locks onto the correct solution for the remainder of the test time. During the initial five minutes the Piksi RTK algorithms are solving the integer ambiguity problem associated with carrier phase measurements. Although this work does not characterize the time it takes for the Piksi algorithms to lock onto the correct solution, the system seemed to lock onto the solution faster when utilizing the better performing GPS antennas.

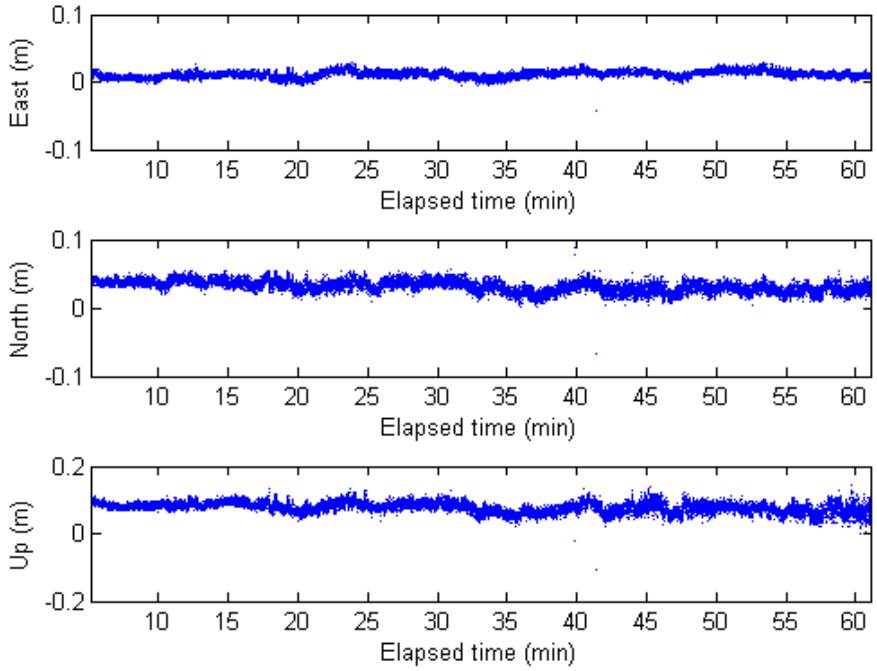


Figure 4-18: Test #1 position solution error during RTK lock

The position solutions are off by a fixed bias to the signal, but it is still under the 10 centimeter accuracy noted by Swift Navigation. Table 4-10 and Table 4-11 show the computed error statistics during Test #1 during the portion of the test that the Piksi was locked onto the RTK solution.

Table 4-10: Test #1 Statistics

| | **East** | **North** | **Up** |
|---|---|---|---|
| Mean Error (m) | 0.011 | 0.031 | 0.078 |
| Standard Deviation (m) | 0.005 | 0.008 | 0.016 |

Table 4-11: Test #1 accuracy and precision measures

| **Measure** | **Value (m)** |
|---|---|
| DRMS | 0.035 |
| MRSE | 0.087 |
| $\sigma_{2D}$ | 0.009 |
| $\sigma_{3D}$ | 0.019 |

The statistics show that during Test #1, the RTK solution was nearly as precise as the solutions during the zero baseline tests. The accuracy, however, was notably decreased relative to the zero baseline tests.

Test #5 showed a significant limitation of the Piksi RTK system. Figure 4-19 is a plot of the position solutions in a local-level East-North coordinate frame centered at the base antenna's location.

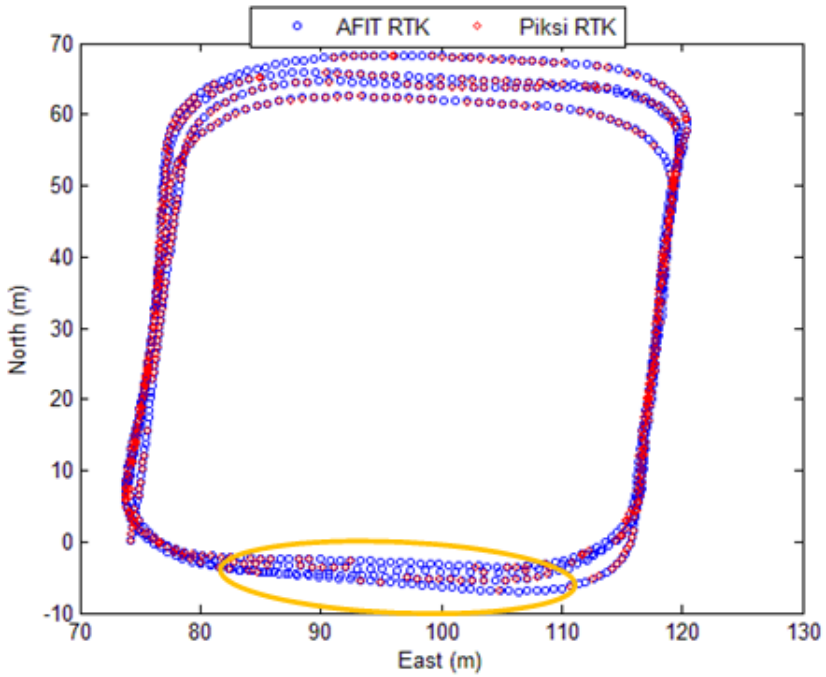


Figure 4-19: Test #5 position solution in East-North frame

The plot shows that the mobile receiver antenna was moved in a box pattern for four laps. The circled area of the plot shows that during portions of the test, the Piksi RTK system, represented by red diamonds, was not outputting position solutions at the specified frequency. This trend was noted during all of the tests that involved a moving mobile antenna. The implications of this finding will be discussed in more detail later in this chapter with the results of the integration test.

The position solution error plot shown in Figure 4-20 exhibits an interesting relationship between relative speed and the error in the Piksi RTK solution. The left plot shows the position solution errors while the plot on the right is the velocity derived from the position solution.

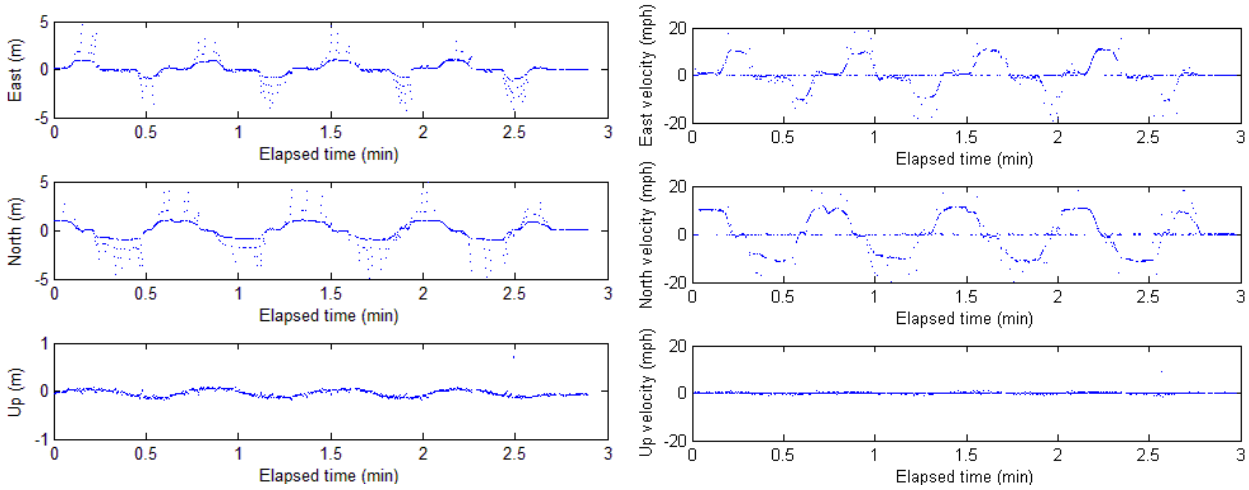


Figure 4-20: Test #5 position solution error and velocity

The plots above show correlation between the velocity of the mobile antenna and the amount of error. As the velocity increase, the error seems to also increase. This is due to the measurement time associated with each position solution from the Piksi RTK system being offset 0.2 seconds relative to the time associated with the position solutions from the AFIT RTK system.

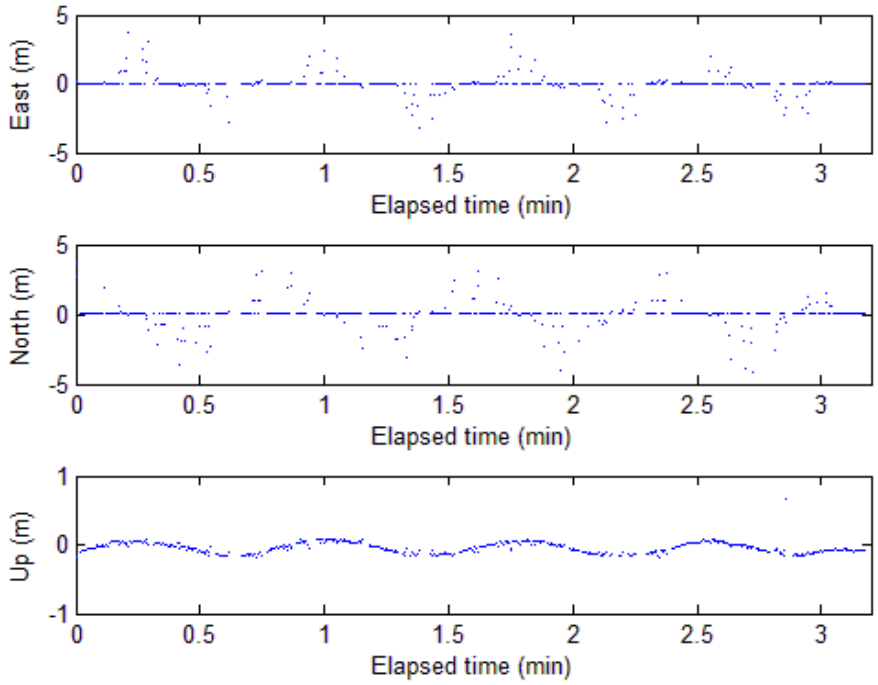


Figure 4-21: Test #5 position solution error after 0.2s offset applied

The remaining spikes in the error plot shown in Figure 4-21 could be mitigated by an outlier rejection algorithm. Rejecting those measurements would, however, further decrease the output reliability of the system.

One other interesting measurement artifact noticed in Figure 4-20 is found on the velocity plots. The data points that are reading zero are directly correlated with the spikes in the error plot to the left. This is caused by the Piksi RTK system outputting several solutions at nearly the same location while the antenna is moving. This is shown in Figure 4-22.

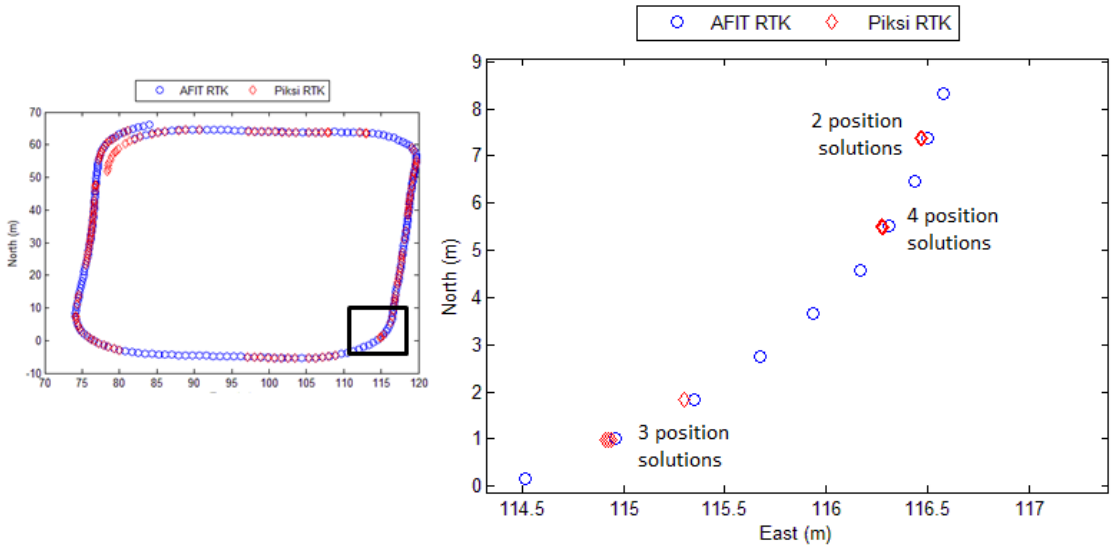


Figure 4-22: Piksi RTK error

The very small change in position solution coupled with the Piksi-reported time difference keeping up with the five hertz collection frequency caused the derived velocity profile to go to zero.

Although the errors from Test #5 do not fit a Gaussian distribution, Gaussian error statistics were computed to show the increased in the error in the Piksi RTK solution. These statistics, which were computed for the data without the 0.2s offset, are found in Table 4-12.

Table 4-12: Test #5 Statistics

| | East | North | Up |
|---|---|---|---|
| Mean Error (m) | 0.034 | -0.066 | 0.043 |
| Standard Deviation (m) | 0.988 | 1.252 | 0.075 |

The implications of this test will be discussed along with the results of the integration test.

The configuration utilized for Tests #2 and #6 could be applied by a user who knows the base position very well but requires position data on a vehicle that cannot carry the larger, high-performance antenna. The tests characterized the Piksi RTK system for application utilizing a known surveyed base location using a high-performance antenna and a mobile receiver using the

Piksi external antenna. A schematic of the test setup utilized in Test #2 is shown in Figure 4-23. For Test #6, the antenna setup was the same as Test #2; however, the golf cart, which houses the mobile antenna, was not stationary throughout the test.

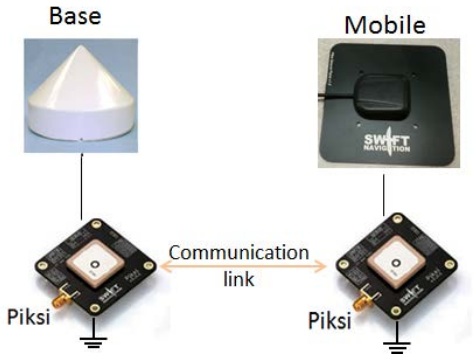


Figure 4-23: Test #2 setup [17] [22]

The algorithms utilized by the AFIT RTK system use measurements from a dual band receiver, causing the AFIT RTK system to not to be compatible with the single band Piksi external antenna. This required the computation of a fixed baseline between the two antennas on the mobile receiver as shown in Figure 3-4. The computed error of the Piksi RTK solution is plotted throughout the entirety of the test in Figure 4-24.

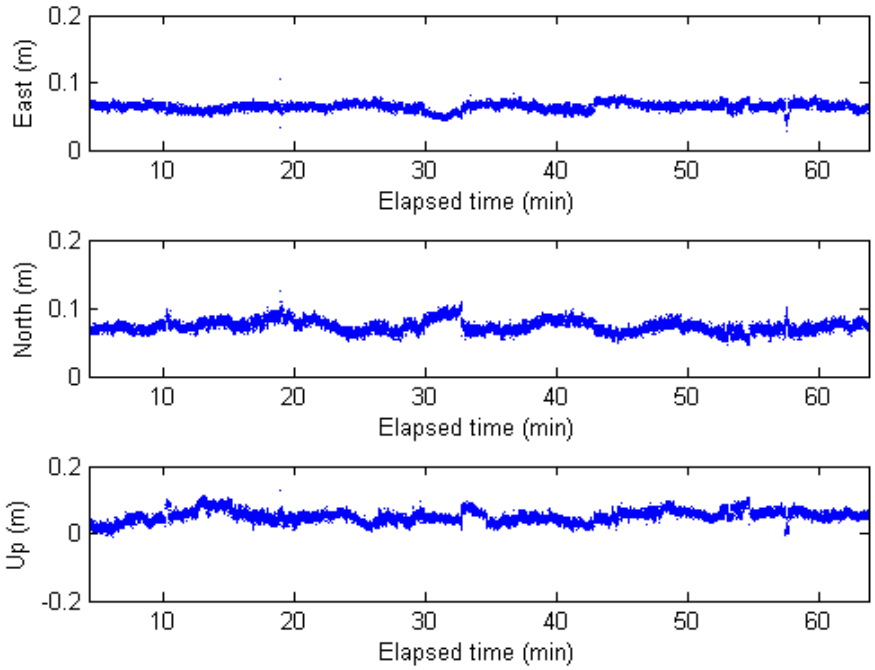


Figure 4-24: Test #2 position solution error during RTK lock

The computed error statistics for Test #2 are found in Table 4-13 and Table 4-14.

Table 4-13: Test #2 Statistics

| | **East** | **North** | **Up** |
|---|---|---|---|
| Mean Error (m) | 0.064 | 0.073 | 0.0511 |
| Standard Deviation (m) | 0.006 | 0.009 | 0.017 |

Table 4-14: Test #2 accuracy and precision measures

| **Measure** | **Value (m)** |
|---|---|
| DRMS | 0.138 |
| MRSE | 0.148 |
| $\sigma_{2D}$ | 0.010 |
| $\sigma_{3D}$ | 0.020 |

The error statistics show that the precision of the Piksi RTK solution is roughly equal to the precision noted during the zero baseline tests. Similar to test #1, the accuracy is off by a bias. Unlike Test#1, this offset in the mean error could have been caused by the method for calculating the offset. For example, changing the measurement of the distance between the two

antennas by a centimeter and heading by three degrees will change the measurement errors by roughly five centimeters.

Because the AFIT RTK system is not compatible with the single frequency Piksi external antenna, measurement error could not be derived for Test #6. The test was run, however, to show how the Piksi RTK system functions using the Piksi external antenna as the mobile antenna. The position solutions, plotted in the East-North local level frame, for one of the four laps of the box pattern are found in Figure 4-25.

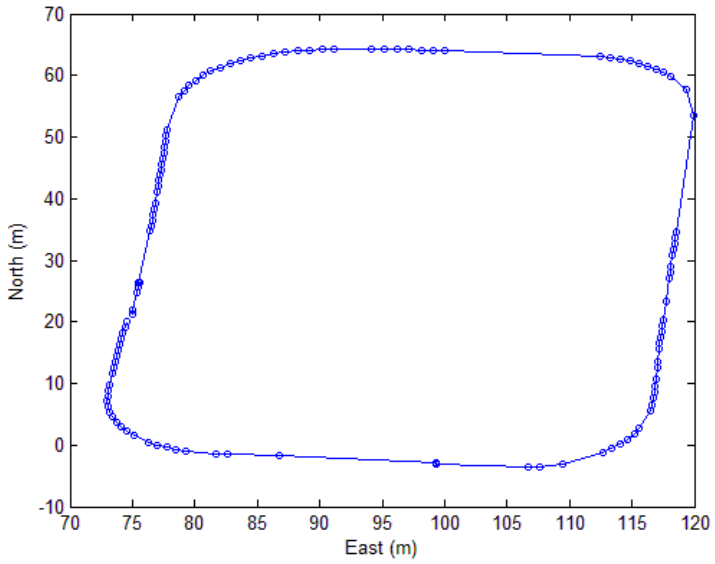


Figure 4-25: Test #6 position solution in East-North frame

The plot shows that the same issues observed during Test #5 were also observed during Test #6.

The configuration utilized by Test #3 and #7 could be applied to a user that only has the capacity to carry a small antenna and does not precisely know their position but require precise relative positions of a vehicle capable of carrying a larger antenna. The test used the Piksi external antenna whose location was determined from the average position solutions and a mobile receiver connected to the NovAtel Pinwheel antenna. A schematic of the test setup

utilized in Test #3 is shown in Figure 4-26. For Test #7, the antenna setup was the same as Test #3; however, the golf cart, which houses the mobile antenna, was not stationary throughout the test.

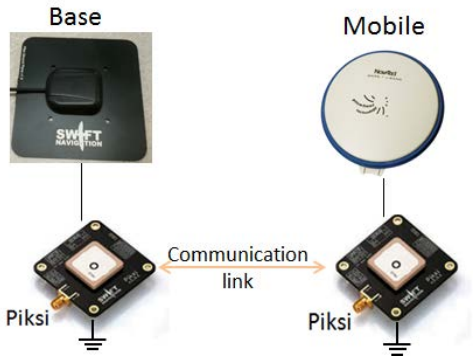


Figure 4-26: Test #3 setup [20] [22]

The method for calculating the error in the position solution was identical to the method used for Test #1 and #5. Figure 4-27 shows the error of the Piksi RTK solution.

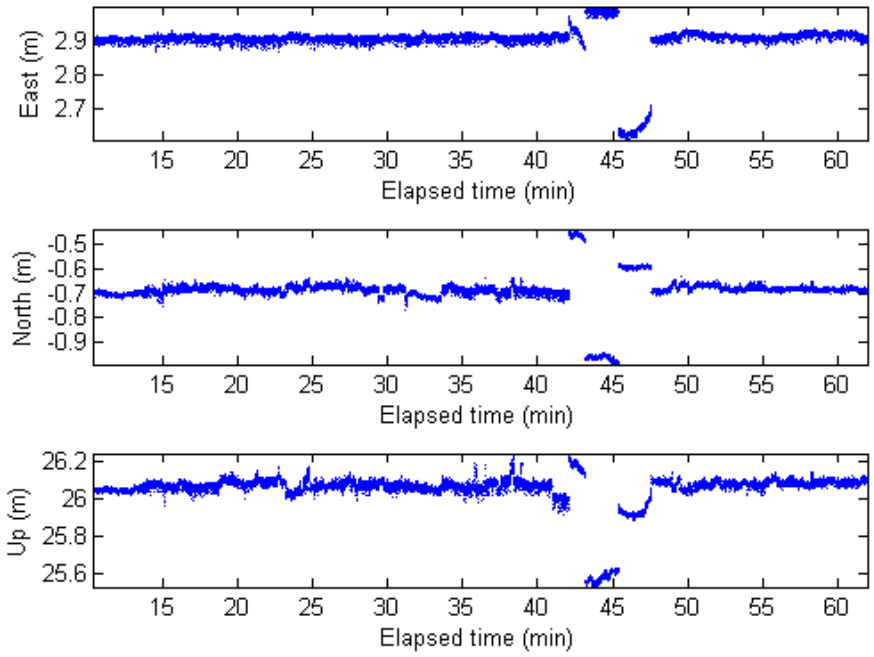


Figure 4-27: Test #3 position solution error during RTK lock

The plot show that there is a large mean error associated with this test configuration. This was caused by using an average absolute position, output by the base Piksi receiver, as the base

position. Because the RTK algorithms output measurements relative to the base position, any error in the base antenna position will translate one-to-one to error in the mobile antenna position. In addition to the offset of the position solutions, at the 42 minute mark the receiver lost its lock on the RTK solution and locked onto several false solutions for a period lasting about five minutes before locking back onto the correct solution. This was not caused by a loss of satellites. The error statistics calculated with and without the data during the five minute period are found in Table 4-15 and Table 4-16.

Table 4-15: Test #3 Statistics

| | **East** | **North** | **Up** |
|---|---|---|---|
| Mean Error (m) | 2.900 | -0.690 | 26.051 |
| Standard Deviation (m) | 0.056 | 0.068 | 0.106 |

Table 4-16: Test #3 Statistics after data removed

| | **East** | **North** | **Up** |
|---|---|---|---|
| Mean Error (m) | 2.906 | -0.689 | 26.070 |
| Standard Deviation (m) | 0.007 | 0.016 | 0.029 |

Table 4-17: Test #3 accuracy and precision measures

| **Measure** | **Value (m)** |
|---|---|
| DRMS | 2.987 |
| MRSE | 26.241 |
| $\sigma_{2D}$ | 0.017 |
| $\sigma_{3D}$ | 0.033 |

The statistics in Table 4-16 and Table 4-17show that the Piksi RTK solution accuracy is severely degraded by the operator relying on the Piksi receiver absolute position measurements to obtain a base position. The precision, however, was not adversely affected.

The plot in Figure 4-28 shows the offset realized in Test #7.

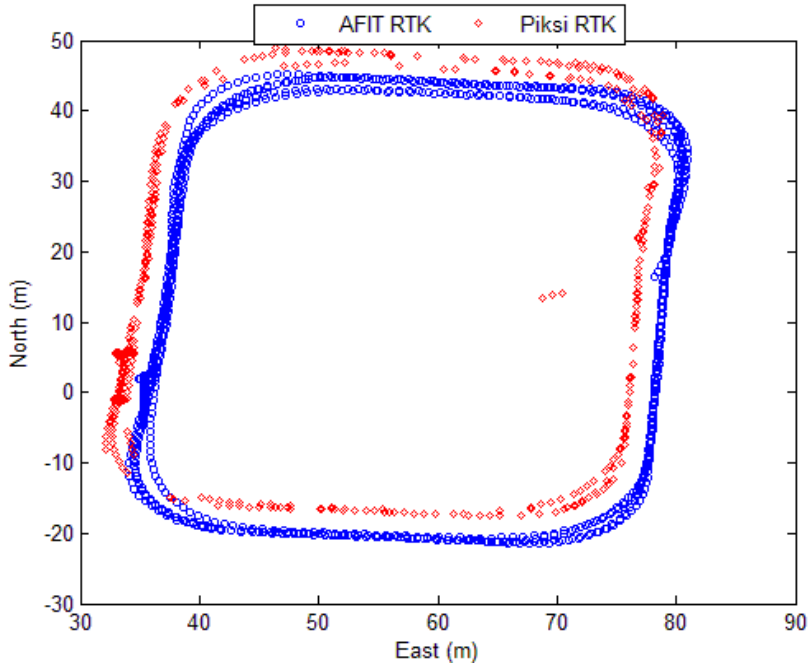


Figure 4-28: Test #7 position solution in East-North frame

As shown in Figure 4-28 a constant, or near constant offset is realized throughout the four laps of the test. Also, similar to Test #1, the position solution error was also directly correlated to the velocity of the receiver. A plot of the position solution error is shown in Figure 4-29.

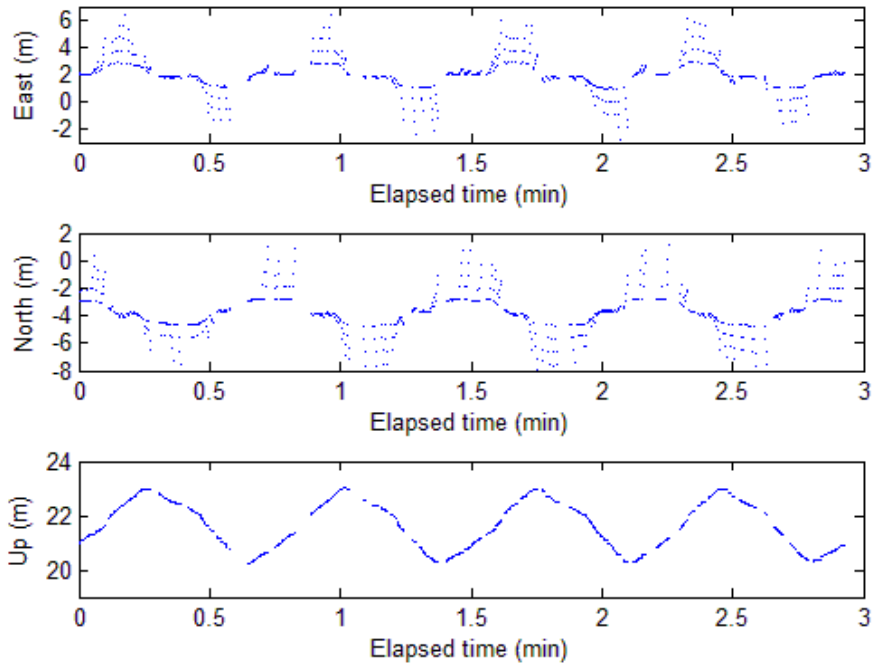


Figure 4-29: Test #7 position solution error

The computed Gaussian error statistics from the Test #7 data are found in Table 4-18.

Table 4-18: Test #7 Statistics

| | **East** | **North** | **Up** |
|---|---|---|---|
| Mean Error (m) | 2.027 | -3.735 | 21.653 |
| Standard Deviation (m) | 1.299 | 1.571 | 0.863 |

The plot of the error in the position solution and table of error show that the in the North and East direction, the Piksi was nearly as precise as the results found in Test #5. The use of the Piksi external antenna as the base antenna increases the precision of the measurements in the Up direction by about a factor of 10.

Similar to Test #5, the relationship between the error and velocity was mitigated by adjusting the time stamp for each of the Piksi RTK system outputs by 0.2 second.

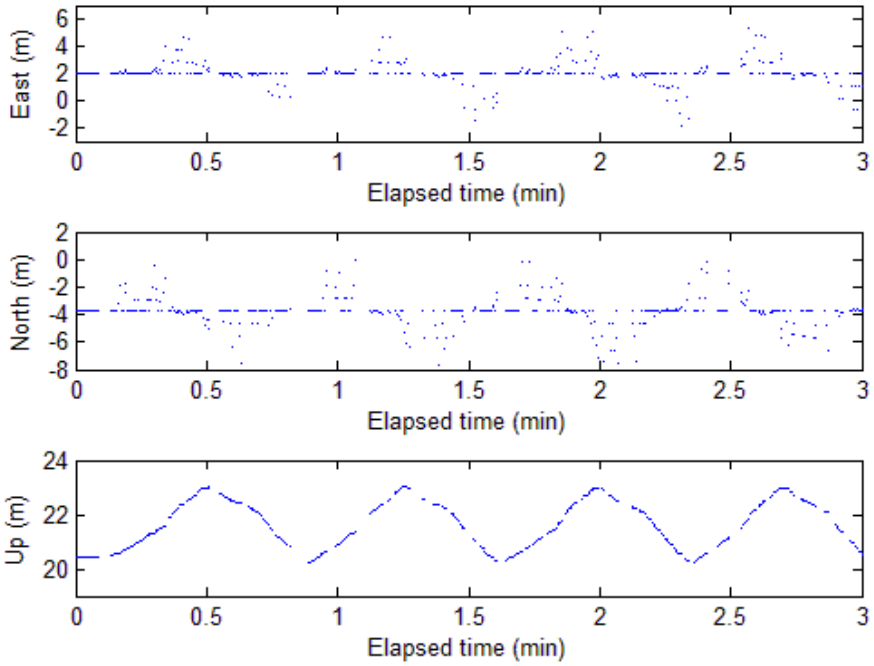


Figure 4-30: Test #7 position solution error after 0.2s offset applied

The configuration utilized by Test #4 and #8 could be applied to a user that only has the capacity to carry a small antenna and does not precisely know their position but require precise relative positions of a small vehicle not able to carry a large antenna. These tests characterize the performance of the Piksi RTK system as if no other hardware is available for use other than the components of the kit supplied by Swift Navigation. A schematic of the test setup utilized in Test #4 is shown in Figure 4-31. For Test #8, the antenna setup was the same as Test #4; however, the golf cart, which houses the mobile antenna, was not stationary throughout the test.

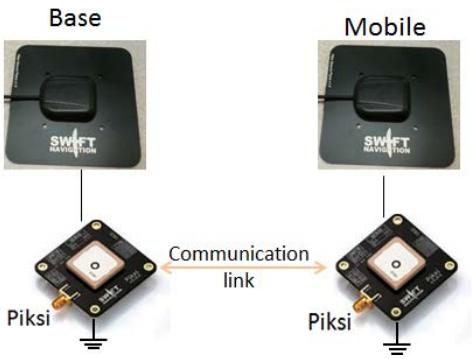


Figure 4-31: Test #4 setup [22]

The calculation of the position solution error for Test #4 was done identically to the error calculated in Test #2. Also, similar to Test #3, the absolute position of the base antenna position was calculated from the average of the output of the base Piksi receiver. The error in the position solution throughout the test time is shown in Figure 4-32.

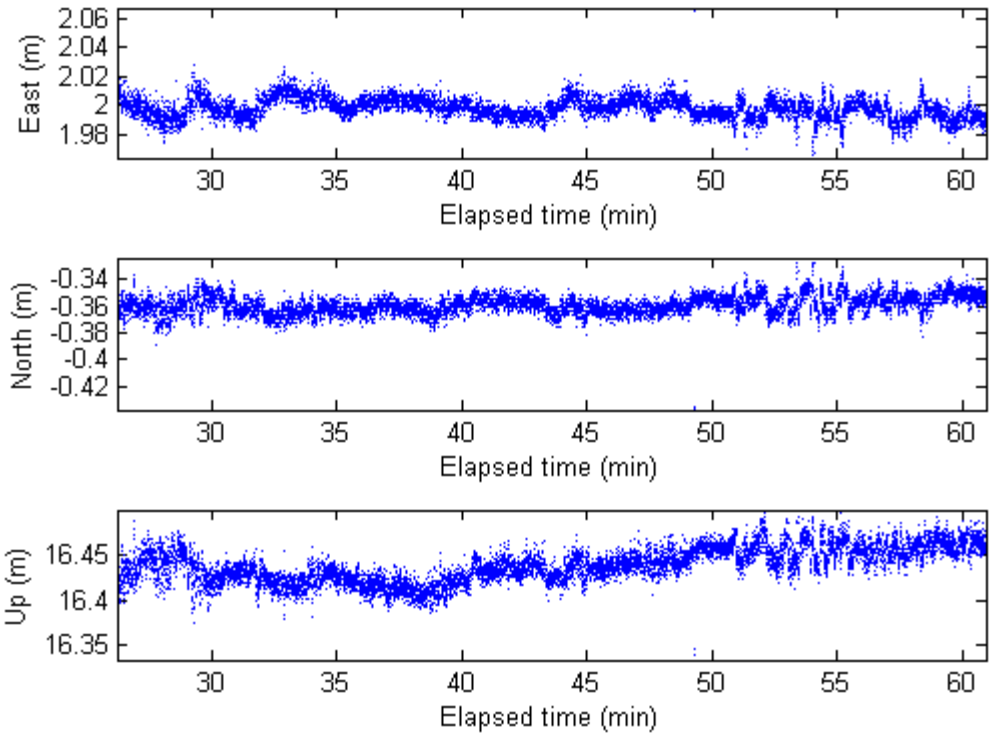


Figure 4-32: Test #4 position solution error

Of note, the RTK lock did not occur until about 25 minutes into the test. This longer wait time for RTK lock was common when utilizing the Piksi external antennas with both the base and

mobile receivers. Similar to other tests utilizing a non-surveyed base antenna location, the position solutions are offset by a fixed bias. This magnitude of this bias is shown in the error statistics found in Table 4-19 and Table 4-20.

Table 4-19: Test #4 Statistics

| | **East** | **North** | **Up** |
|---|---|---|---|
| Mean Error (m) | 1.998 | -0.359 | 16.438 |
| Standard Deviation (m) | 0.007 | 0.007 | 0.019 |

Table 4-20: Test #4 accuracy and precision measures

| **Measure** | **Value (m)** |
|---|---|
| DRMS | 2.030 |
| MRSE | 16.563 |
| $\sigma_{2D}$ | 0.010 |
| $\sigma_{3D}$ | 0.022 |

While the accuracy of the measurements are severely degraded relative to the zero baseline tests, the precision of the Piksi RTK solution does not seem to be appreciably affected by the use of the Piksi external antennas. Similar to other tests utilizing the Piksi external antenna with the base receiver, the decreased accuracy was caused by an inaccurate base antenna position and not a degradation of the baseline measurement accuracy.

The Piksi RTK position solutions from one of four laps, in a local level East-North coordinate frame, are shown in Figure 4-33. Similar to Test #6, a truth source was not available due to the incompatibility of the AFIT RTK system with the Piksi external antenna.

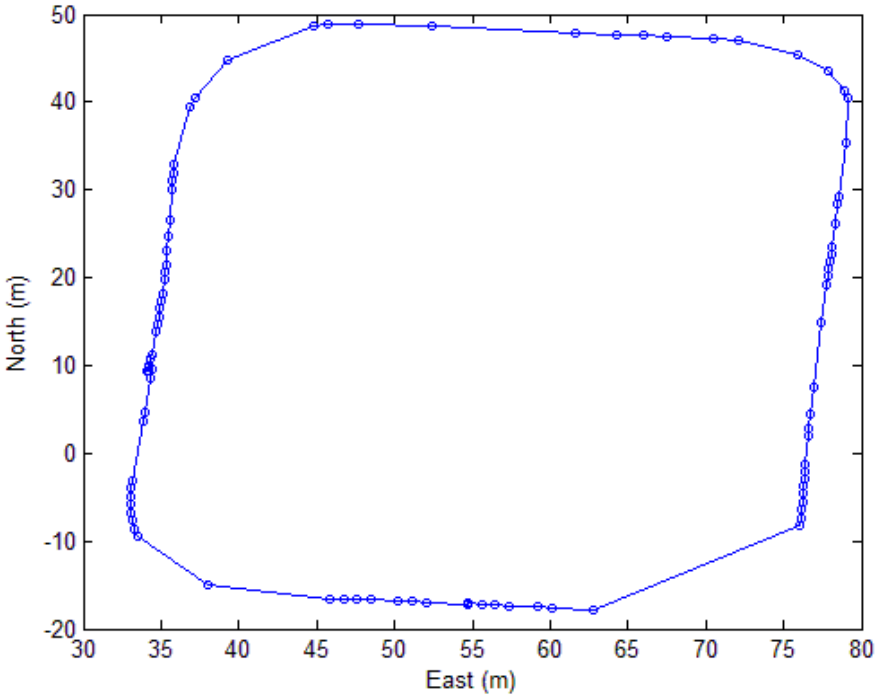


Figure 4-33: Test #8 position solution in East-North coordinate frame

As has been noted in all other test with a non-stationary mobile receiver, the Piksi RTK system did not output solutions at a regular rate. This would limit the effectiveness of the Piksi RTK system were it to be employed by a system such as a UAS that requires regular position solutions.

The final RTK test conducted involved using the Piksi external antenna for the antenna of a zero baseline test connected via an antenna splitter to Piksi receivers. The antenna and both receivers were then placed on a mobile platform to determine the relative positioning error of the Piksi RTK system while both the base antenna and mobile antenna are in motion. A schematic of the setup for this test is found in Figure 4-34.

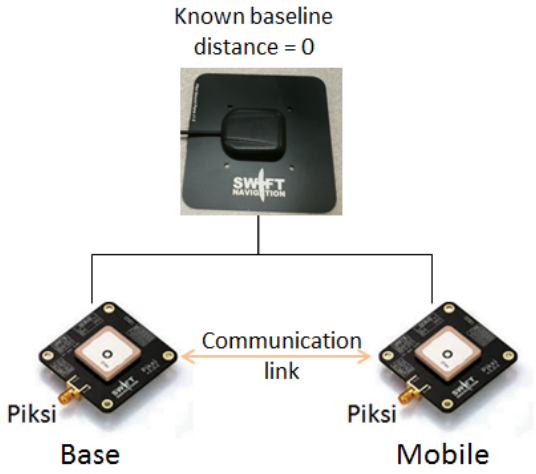


Figure 4-34: Mobile zero baseline test [22]

This test simulates an application in which only relative positions are required by the system. All configuration settings were kept constant except for the mode change from "Low Latency" to "Time Matched". This setting, according to the Piksi datasheet, changes how often the observations from the base receiver are sent to the mobile receiver [22]. A plot of the error throughout the test duration as well as the relative position of the AFIT RTK antenna is shown in Figure 4-35.

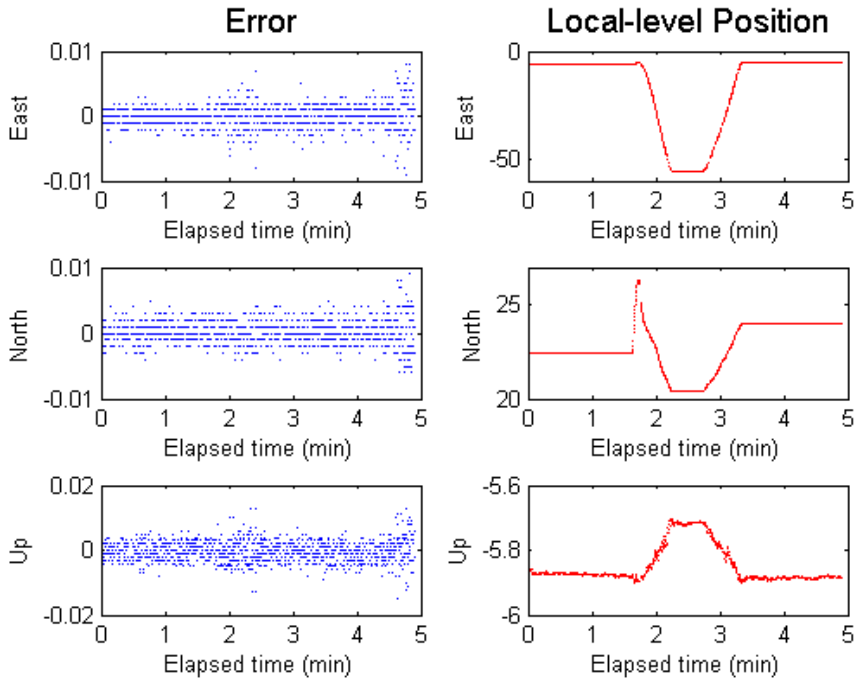


Figure 4-35: Position solution error

Figure 4-35 shows that even while the platform is in motion, the accuracy and precision of the Piksi RTK baseline solution is unaffected. Error statistics from this test, found in Table 4-21, show the statistics match the computed statistics from the zero baseline tests.

Table 4-21: Moving Base Antenna Test Statistics

| | **East** | **North** | **Up** |
|---|---|---|---|
| Mean Error (m) | < 0.001 | < 0.001 | < 0.001 |
| Standard Deviation (m) | 0.002 | 0.002 | 0.003 |

The mode was then changed back to the "Low Latency" mode and the tests were re-accomplished. Figure 4-36 shows that the error in the Piksi RTK baseline for this test had similar trends to Test#5 and #7. These errors, however, could not be mitigated by applying an offset to the time stamp.

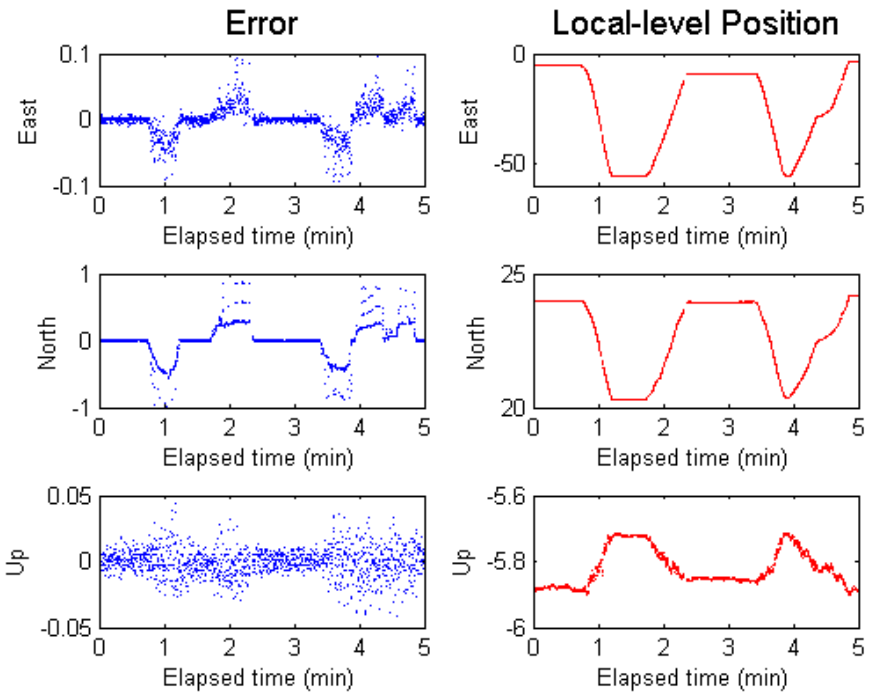


Figure 4-36: Position solution error

The limitation for the 'Time Matched' mode is that the Piksi system cannot keep up with the specified output frequency. In other words, if the operator sets the output frequency to five hertz, the Piksi system will miss several outputs before a solution is output. This limitation is also present while the mode is set to "Low Latency", but it is much more prevalent when the mode is set to "Time Matched". A plot showing the time difference between consecutive samples is shown in Figure 4-37. The output frequency was set to five hertz, or 0.2 seconds time difference.

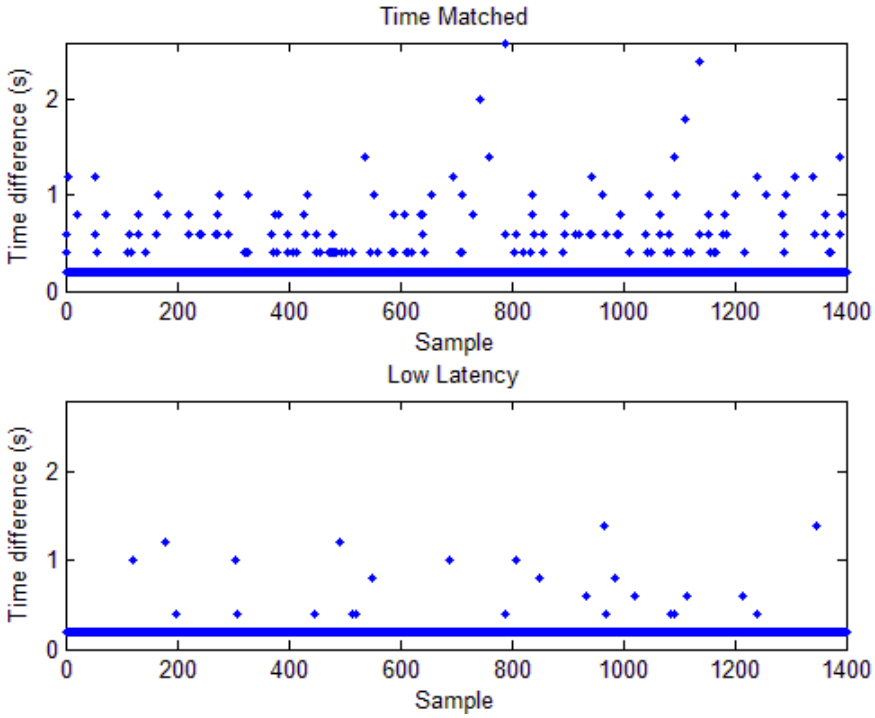


Figure 4-37: Output frequency comparison

The plot shows that while the Piksi system's mode is set to "Time Matched" the reliability of the Piksi outputting a solution at the correct frequency is about 5 times less than while the system's mode is set to "Low Latency". The output reliability of the "Time Matched" test was found to be 90% versus the 98% output reliability during the "Low Latency" tests.

The RTK GPS tests have shown the expected accuracy and precision for several antenna configurations. Results from these tests could be used by perspective users of the Piksi RTK system to show system performance under varying conditions. The next section will address how the Piksi RTK system responds to external factors common on small UAS.

**Integration Test**

The integration tests were conducted to show how the Piksi RTK system performs in conditions common on small UAS without flying the system on a UAS. The two tests that were conducted were vibration tests and simulated flight tests. The configuration of the Piksi

receivers for all integration tests was kept constant and match the manufacturer's recommended setup. For the vibration test the base receiver was mounted to an isolated platform while the mobile receiver was mounted to the shaker table. . As stated in Chapter 3, the frequency of the vibration was varied from 40 to 200 hertz in 10 hertz increment each minute while the amplitude was held constant at 2.5 millimeters. The test was conducted three times, once per orthogonal axis. The resulting baseline position solution error is found in Figure 4-38.

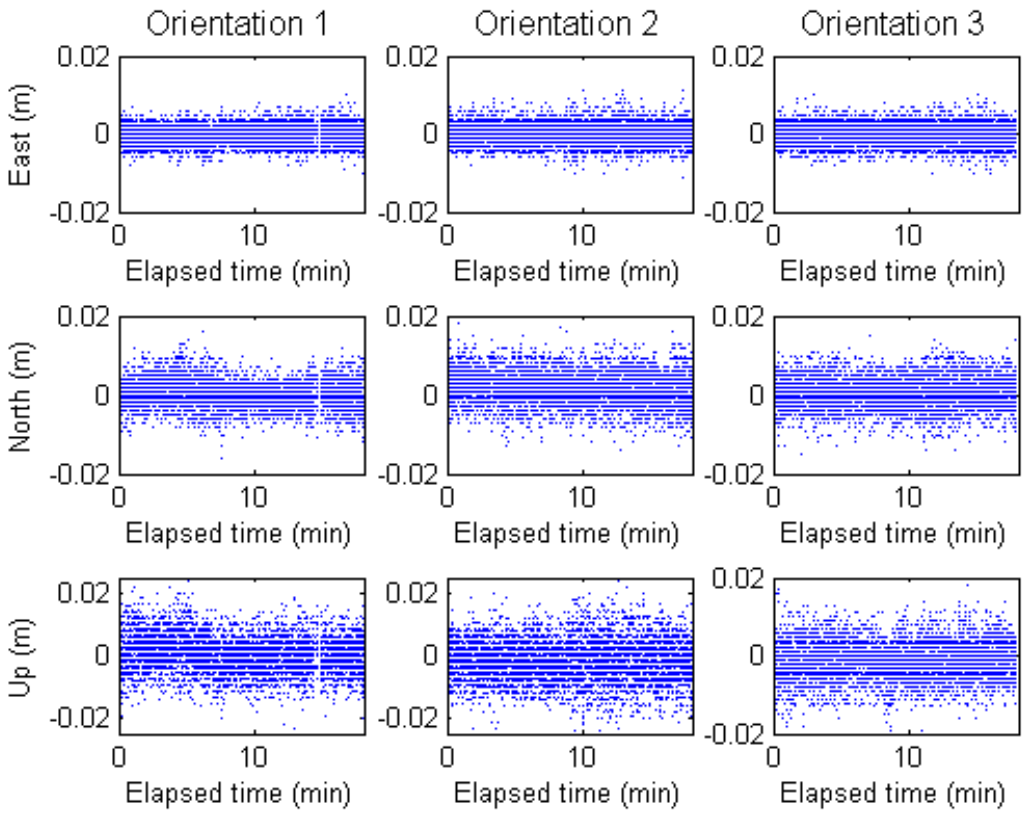


Figure 4-38: Position solution error during vibration test

Figure 4-38 shows that the Piksi RTK system was not affected by the external vibrations ranging from 40 to 200 hertz at 2.5 millimeters amplitude.

The simulated flight test, as described in Chapter 3, attempted to expose any limitations of the Piksi RTK system to having the GPS antenna mounted to a rolling aircraft. The test also

showed how the Pixhawk autopilot works with input from two, independent, GPS receivers. These results will help users of the Piksi system become more familiar with the limitations. The robustness of the Piksi RTK solution to the rolling aircraft was characterized by examining the GPS status reported by the Pixhawk autopilot. For the test, the simulated UAS was driven in a box pattern followed by a zigzag pattern. During each of the turns, the simulated aircraft was rolled to simulate the rolling motion of an aircraft. A status greater than 3 relates to a differential GPS solution. Figure 4-39 shows the roll, pitch and yaw as they are output from the autopilot along with the GPS status.

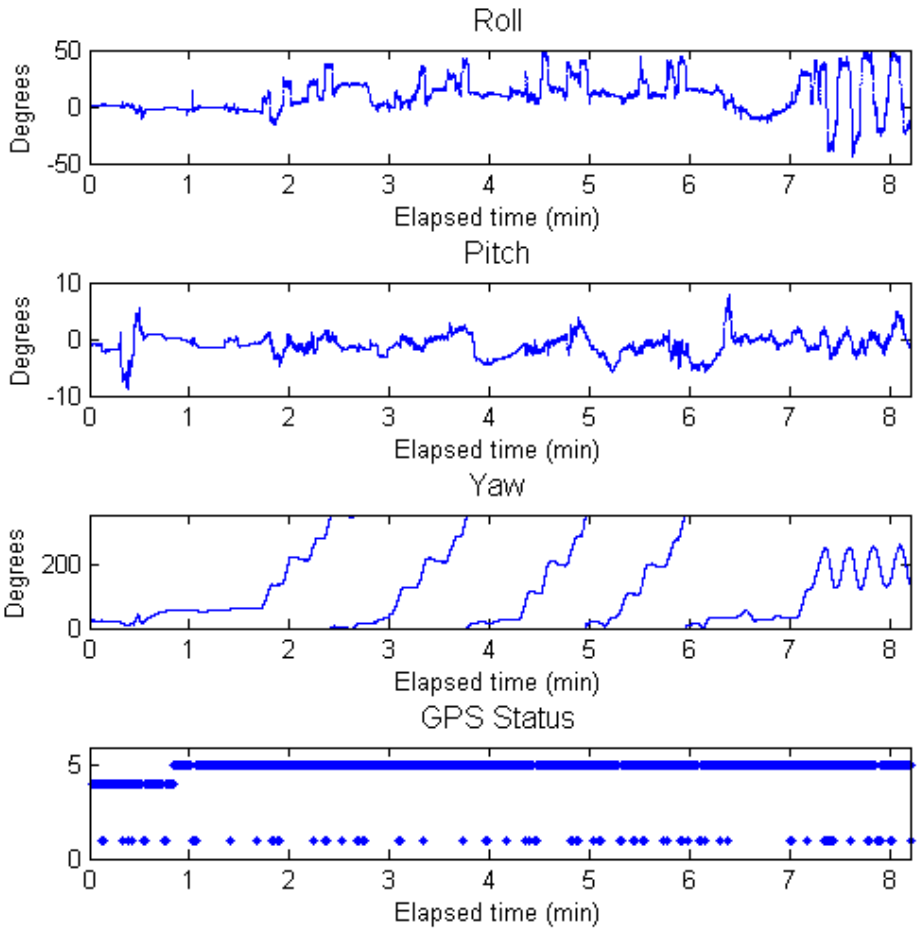


Figure 4-39: Piksi GPS status

The figure shows that throughout the test the Piksi RTK system maintained its lock on the RTK solution. While the test displays the robustness of the Piksi RTK system to account for satellites coming in and out of view, it should be noted that the success of the test is highly dependent on the location of the GPS satellites in view. Up to eight GPS satellites were reported by the Piksi receiver throughout the test. If this number had been 4 or 5, the results of the test would likely have been different.

The position solutions from the 3DR GPS receiver, Piksi receiver and the outputs from the Pixhawk's extended Kalman filter (EKF) were analyzed to show how the Pixhawk EKF handles the multiple inputs. The EKF within the Pixhawk autopilot takes inputs from the sensors on board the UAS, such as accelerometers and gyroscopes, and outputs a position, velocity and vehicle orientation solutions in a local-level coordinate frame centered on the first GPS solution output from the primary GPS receiver [2]. Figure 4-40 is a plot of the position solutions from the Piksi RTK system, 3DR GPS receiver and the EKF solution plotted in the local level coordinate frame. The center of the local level frame is the first position solution from the received by the Pixhawk autopilot from either of the GPS receivers.

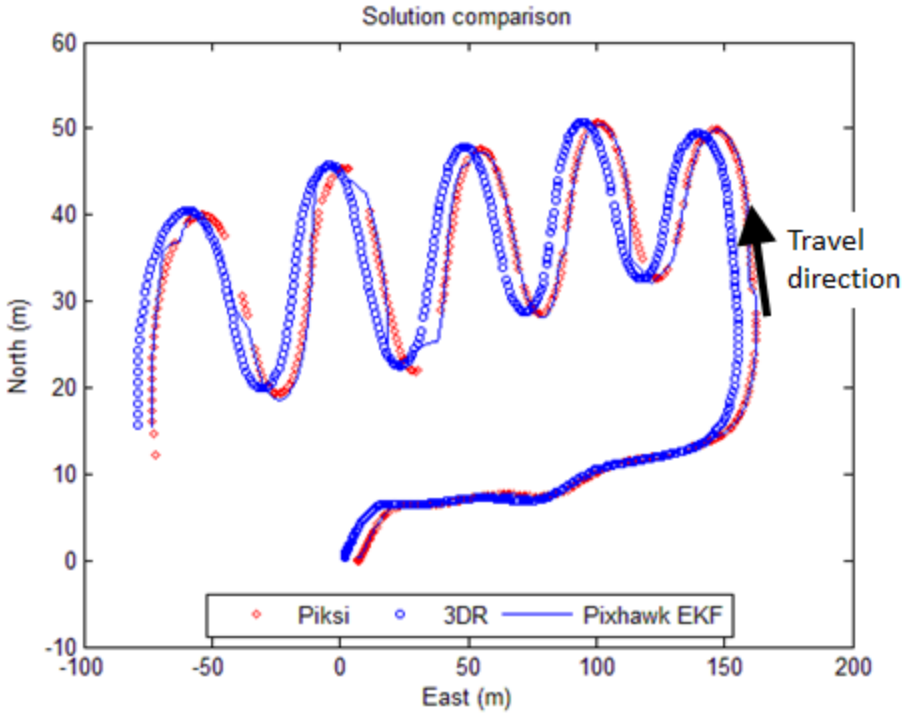


Figure 4-40: Solution comparison

The plot shows a constant offset which was also prevalent in the RTK GPS tests between the Piksi solution and the 3DR solution. This is caused by an inaccurate base Piksi antenna position. Even though the 3DR solution was shown to be more accurate than the Piksi, the EKF closely follows the Piksi's solution because it is reporting a higher GPS status. Figure 4-41 shows how the EKF handles situations when the Piksi is not outputting solutions at the specified five hertz rate.

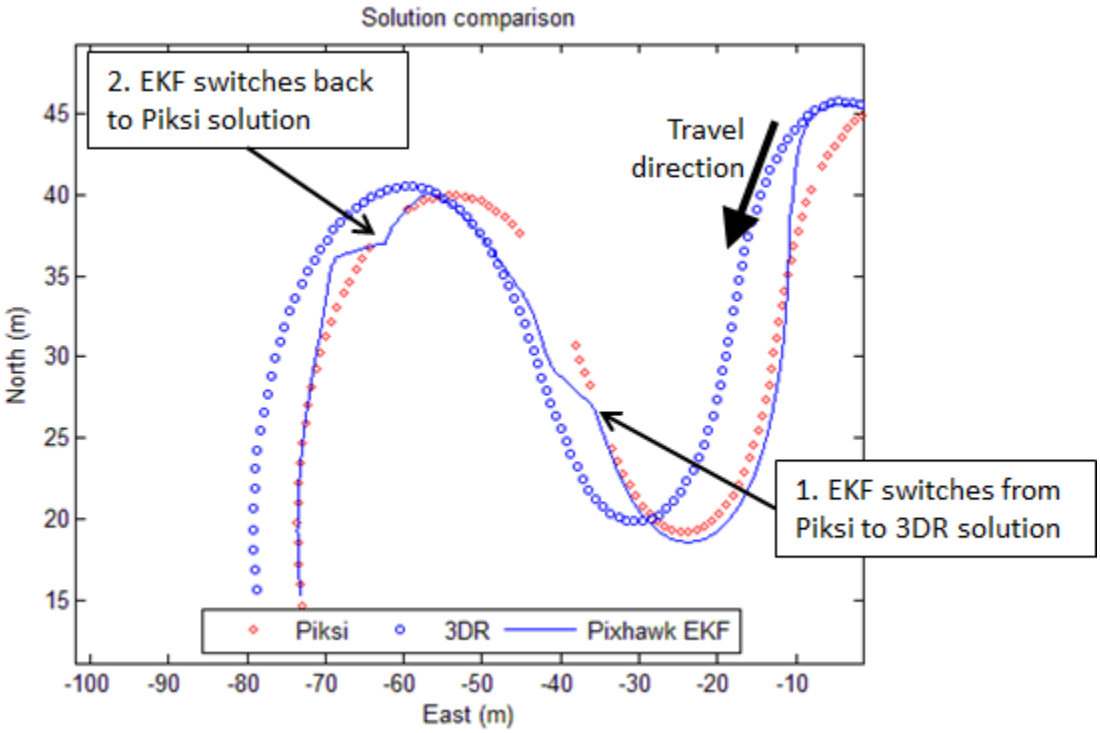


Figure 4-41: Solution comparison close-up

The figure shows that for a short period of time after the Piksi stops reporting position solutions at the regular interval the EKF resorts to the 3DR solution, even when the Piksi reports four consecutive solutions. Then, after the Piksi has resumed outputting measurements, the EKF switches back to the Piksi solution. The interval period that the autopilot software waits before switching is not tunable at this time [2]. Unless, the reliability of the Piksi system is upgraded, this is a limiting factor for use of the Piksi system in UAS applications.

**Potential Applications**

The outputs from the Piksi RTK system testing can be used to suggest several applications. Along with applying the Piksi RTK system for UAS applications, the agriculture industry is also a potential application. In the late-1990s Navcom Technology, Incorporated, a component of John Deere and Company, implemented a differential GPS service called, StarFire™, specifically tailored for farming applications [16]. The system consists of a series of

ground stations, used to calculate differential offsets, and geosynchronous satellites that distribute the information to user equipment [16]. The accuracy required by farming operations is well within the accuracy and precision observed by the Piksi RTK system. Operations such as bulk fertilizer application, cultivating and harvesting require two-sigma horizontal position accuracy from 46 down to 5 centimeters [12]. While, the Piksi RTK system may not be able to achieve the 5 centimeters of accuracy, the system is capable of the producing baseline measurement accuracy within the specifications for many other agricultural applications.

The primary limiting factor for applying the Piksi RTK system is the integration with the farming equipment. The equipment manufactured by Navcom, has the advantage of being designed by a component of the company that manufactures the farming equipment, John Deere. This allows the receivers and to be highly cohesive with the vehicle control system. Integrating the Piksi system would require decoupling the Navcom equipment from the vehicle control system and then integrating the Piksi RTK system.

Another application for the Piksi RTK system is for use with a cooperative control architecture employing multiple UAS. For these architectures, information on the relative distance between the vehicles is more important than the absolute location of each of the vehicles. Since the Piksi system contains its own processing, the amount of coupling between the RTK algorithms and the flight control algorithms onboard the flight controller would be minimal. Work would be required to determine how to get the outputs of the baseline measurements from the Piksi system to the flight controller. The key limitation for utilizing the Piksi RTK system for this application is the output reliability. This would limit the cooperative control architecture from being applied to operations involving close formation flight or high speed vehicles.

One final application for the Piksi RTK system to be discussed is the use of the system as a truth source for further small UAS research. As discussed in Chapter 1, the Air Force Institute of Technology has been conducting research with small UAS for many years. Before the Piksi system was commercially available, research regarding new navigation algorithms utilized the 3DR GPS kit as a truth source because of its low cost, small size and ease of integration. The drawback, however, it the precision of the measurements output by the system. As was shown when comparing the results from the short baseline test of the 3DR GPS kit to RTK GPS Test #2, the Piksi system outperforms the 3DR GPS kit by a factor of 100. Although the price of the Piksi RTK system is much higher than the 3DR GPS kit, the cost is low enough and the components are small enough to be applied to further AFIT research.

In order to take advantage of the high accuracy of the Piksi RTK system, a higher cost GPS receiver and antenna combination in, such as the ones used in this research as the truth source, should be utilized to determine the position of the base antenna. Although the zero baseline test of the Piksi receiver as a standalone receiver showed that the error is very low, the data was collected over a time span of 24 hours. The RTK GPS Tests utilizing the Piksi antenna connected to the base receiver noted a severe degradation in the accuracy of the baseline measurements. In the field where testing is conducted, the collection of 24 hours of data before testing can occur is not a feasible solution, therefore it is recommended that a higher cost receiver and antenna combination be utilized to determine the base position. The higher cost antenna can then also be utilized as the base antenna with the Piksi RTK system.

**Summary**

This Chapter has shown the effectiveness of the Piksi system as both a standalone GPS receiver and a high precision RTK system. It was shown that when operating as a standalone

receiver, the absolute position measurements were less accurate and precise than both the NovAtel reference receiver and 3DR GPS receiver. The RTK system tests showed how well the Piksi RTK system performs the task it was designed to do: deliver high accuracy and precision relative positions. The results showed that the accuracy of the Piksi is less than 3 millimeters in a lab setting. For static tests, in an operational setting, the accuracy measures were about 18 millimeters as shown in RTK GPS Test #1. The limitations of the Piksi RTK system were realized when examining the position error from tests involving a non-stationary mobile antenna. The data shows that the system's position error increases with the velocity of the antenna if the an offset is not applied to the timestamp. For the test when both the base and mobile antenna were moving, this error was mitigated by switching the mode to "Time Matched". Changing this configuration setting, however, exacerbates an additional limitation uncovered during the testing. The reliability of the Piksi RTK system outputting a measurement at the commanded rate was found to be an issue. Figure 4-37showed that over the span of the test, the output reliability was only 90% while the system was in "Time Matched" mode versus the 98% exhibited in "Low Latency" mode.

Integration tests showed that the Piksi RTK system is unaffected by the range of external vibrations that receiver was exposed to. To further shows the effect of being integrated into a UAS would have on the Piksi RTK system, the simulated UAS test showed how the Pixhawk autopilot works with the Piksi system. When the Piksi system does not provide a solution the EKF running on the Pixhawk autopilot uses inputs from a redundant GPS receiver.

This chapter concluded with briefly discussing the potential applications of the Piksi RTK solution. The data within this research has shown that while there are issues with the Piksi RTK system, AFIT would benefit by implementing the Piksi RTK system on their small UAS

platforms to use as a truth source when proving new navigation methods. The next chapter will use the results found in this chapter to answer the investigative questions found in Chapter 1.

# 5. CONCLUSION

This Chapter will address the investigative questions posed in Chapter 1 that guided the research effort. The Chapter will conclude with recommended areas for future work.

## Investigative Questions Revisited

After briefly discussing the background and research objectives, Chapter 1 posed a series of investigative questions. This section will address those questions and give some insight into why those questions are relevant to the Air Force Institute of Technology.

What is the accuracy of the current hobbyist hardware configuration?

This investigative question is answered by this work to aid other researchers using common hobbyist components on their research as well as provide a baseline to compare to the Piksi RTK system. This research specifically investigated the accuracy and precision of the 3DR GPS receiver kit [1]. Although there is documentation regarding the accuracy and precision of the uBlox receiver integrated into the 3DR kit, information regarding how well the kit performs with the integrated antenna had not been completed.

The results of the data collection showed that accuracy of the 3DR GPS receiver kit has DRMS of 1.58 meters and MRSE of 3.08 meters. The two and three dimension precision statistics were computed to be 1.56 meters and 4.26 meters, respectively. These values help to explain why Lt Stefan Hardy, whose thesis investigated COTS formation flying algorithms, realized errors around 5 meters [11].

How can the RTK-GPS system be implemented into existing UAS architectures?

This is a fundamental question for any enterprise when a new piece of equipment is purchased. The performance of the Piksi RTK system as a standalone system works very well in certain applications. This question asks how the system should be implemented into an existing UAS architecture. The integration tests showed that the Piksi system works well with the existing equipment available to the hobbyist community. There are several considerations to be addressed by the user before integrating the system. One consideration is how to address the time offset noticed during the RTK test. This is not an issue if the user is only worried about the absolute position of one Piksi relative to the other, but it will present an issue if a different type of receiver is used.

Another consideration is the output reliability issue. Changing the mode from "Low Latency" to "Time Matched" decreased the output reliability of the system, as described in Chapter 3. The low output reliability of the system requires that the Piksi RTK system to be utilized in a system that contains a redundant source of position information. The Pixhawk autopilot allows for a redundant GPS receiver along with embedded inertial measurement sensors to be used that provides the system with position measurements if and when the Piksi does not output solutions. The GPS switching was shown during the integration test.

One final consideration for implementing the Piksi RTK system into an existing UAS architecture is the communication subsystem within the Piksi system. Many UAS that employ autopilots for autonomous or near autonomous navigation utilize a telemetry communication link from a ground station computer to the autopilot. The standard communication frequency utilized for this telemetry is the same frequency used by the communications modems supplied with the Piksi RTK system. This requires the user of the system to configure the pairs of communication

modems on separate channels or have one pair utilize the upper portion of the spectrum while the other uses the lower portion. Either way, the setup of the communication architecture is important for allowing the telemetry link and the Piksi communication link to work properly.

How accurate and precise are the low-cost RTK systems?

The accuracy and precision of the Piksi RTK system being investigated was done in through a series of tests. By their nature RTK position solutions are in a relative coordinate frame instead of the absolute frame. To obtain absolute accuracy the Piksi RTK system a known base antenna location was determined. The relative position baseline was then added to the base location to obtain position solutions of the mobile antenna in an absolute coordinate frame. For the static tests that utilized an antenna located at a surveyed location, the Piksi RTK system displayed a DRMS of 0.035 meters and MRSE of 0.087 meters. The two and three dimensional precision of the Piksi RTK system was found to be 0.007 meters and 0.014 meters, respectively.

As shown RTK GPS Test #5 and #7 the accuracy and precision of the Piksi RTK system is drastically reduced if the mobile antenna is moving. These tests showed that the error in the baseline position was increased while the mobile antenna was moving. Once a 0.2 second offset is applied to the time stamp the accuracy improves, but is still not as accurate as the stationary tests showed. The DRMS and MRSE found during Test #5 after the 0.2 second offset was applied were found to be 1.024 m and 1.028 meters, respectively. This is not much better than the 3DR GPS kit. Characterization of this error as a function of speed was not conducted, but it was clear from the data that movement in the East direction caused as increase in the error in the baseline measurement in the East direction with no increase error in the other axis.

What are the limiting factors associated with the low-cost hardware versus the traditional hardware?

In addition to the limitations discussed above, increased error and output reliability, the time required for the Piksi system to start outputting RTK solutions and absolute position accuracy and precision are limitations present in the Piksi system that are not present in traditional, higher cost, hardware. The time required before the Piksi starts outputting the high precision measurements was not systematically quantified in this research. Examining the data logs from the RTK GPS tests shows that time was five to ten minutes on average. This time is much higher than the RTK system discussed in Chapter 2, the SBG Ellipse-D, which takes less than 50 seconds and the AFIT RTK system utilizes the NovAtel DL-V3 which requires 60 seconds [18][20]. This limitation discussed briefly with the results to RTK GPS Test #1 increase the setup time of the UAS. Since the Piksi system does not require user input during this time, the user could be conducting other setup-related tasks.

The absolute accuracy and precision of the Piksi receiver as a standalone is a limiting factor that was very prevalent during the RTK GPS tests utilizing the Piksi external antenna connected to the base receiver. For these tests, the base position was calculated based on the average absolute position measurement output by the base Piksi receiver. The results of the test showed that the average error for those tests, the average error was much higher than the tests utilizing an antenna at a known, surveyed location. This shows the error of using a relative positioning system to obtain results in an absolute coordinate frame. If the application of the Piksi system does not require the conversion of the relative baseline position to an absolute position, than these errors would be equal to the errors found during the test utilizing the surveyed base antenna location. One potential application for this system would be integrating

the system on a set of UAS that require maintaining a formation. In this application, the absolute position of the individual aircraft is not as important as the relative distances between them.

**Recommendations for Future Work**

One suggested objective for future research is to implement the Piksi RTK system on a UAS to demonstrate the integration discussed in this research. Additional characterization of the Piksi RTK system's error statistics will also require the integration of a truth source onto the UAS; preferably utilizing the same GPS antenna as the Piksi receiver.

The Piksi RTK system could also be integrated into a UAS architecture designed for cooperative control such as the one utilized by Lt Stefan Hardy. Re-accomplishing the accuracy test conducted within the Hardy thesis would show the increased accuracy achieved by implementing the Piksi RTK system.

One final area left unaddressed by this research is fully optimizing the Piksi RTK system for a specific mission. There are a number of configuration settings both on the Piksi and on the Pixhawk autopilot that will affect the performance of the system. This RTK GPS test portion of this research attempted to give results for a wide variety of applications of the system, but left the configuration of the Piksi constant.

# WORKS CITED


1. 3DR. “3DR uBlox GPS with Compass Kit.” https://store.3dr.com/products/3dr-gps-ublox-with-compass. [Accessed 15 January 2016]

2. 3DR. “Extended Kalman Filter Navigation Overview and Tuning.” http://dev.ardupilot.com/wiki/extended-kalman-filter/. [Accessed 21 January 2016]

3. ARINC Research Corporation. Navstar GPS Space Segment / Navigation User Interfaces. ICD-GPS-200, 12 April 2000.

4. Bouska, Terry J. Development and Simulation of a Pseudolite-Based Flight Reference System. MS Thesis, AFIT/GE/ENG/03-03. School of Electrical Engineering, Air Force Institute of Technology (AU), Wright-Patterson Air Force Base OH, March 2003 (ADA415247).

5. Comstock, Stephen J. Development of a Low-Latency, High Data Rate, Differential GPS Relative Positioning System for UAV Formation Flight Control. MS Thesis, AFIT/GCS/ENG/06-12. School of Electrical Engineering, Air Force Institute of Technology (AU), Wright-Patterson Air Force Base OH, September 2006 (ADA456888).

6. Department of the Air Force. Small Unmanned Aircraft Systems Training. AFI 11-502v1. Washington: HQ USAF, 26 April 2012.

7: Emlid. "Reach: High accuracy L1 RTK GNSS." http://www.emlid.com/reach/. [Accessed 22 January 2016]

8. Federal Aviation Administration. "Pilot Reports of Close Calls With Drones Soar in 2015." https://www.faa.gov/news/updates/?newsId=83445. [Accessed 22 January 2016]

9. Gakstatter, Eric. “RTK GNSS Receivers: A Flooded Market.”Available: http://gpsworld.com/gtk-gnss-receivers-a-flooded-marker/. [Accessed 28 July 2015]

10. “Global Positioning System.” 11 February 2014. [Online]. Available: http://www.gps.gov/systems/gps/. [Accessed 11 August 2015]

11. Hardy, Stefan L. Implementing Cooperative Behavior & Control Using Open Source Technology Across Heterogeneous Vehicles. MS Thesis, AFIT/ENV/MS-15. Department of Systems Engineering, Air Force Institute of Technology, Wright-Patterson AFB, OH, March 2015 (ADA616324).

12. Hatch, Ron, Tenny Sharpe, and Paul Galyean. “ StarFire: A Global High Accuracy Differential GPS System”. Proceedings of the 2003 National Technical Meeting of The Institute of Navigation. 562-573. 2003.

13. Keane, J. F. and S. S. Carr. “A Brief History of Early Unmanned Aircraft”. Johns Hopkins APL Technical Digest, 32 (3): 558-571, 2013.

14. Kickstarter. "Piksi : The RTK GPS Receiver." https://www.kickstarter.com/projects/swiftnav/piksi-the-rtk-gps-receiver. [Accessed 22 January 2016]

15. Misra, Pratap and Per Enge. Global Positioning System: Signals, Measurements, and Performance (2nd Edition). Lincoln: Ganga-Jamuna, 2011.

16. Navcom Technologies Incorporated. "StarFire™". https://www.navcomtech.com/navcom_en_US/products/equipment/cadastral_and_boundary/starfire/starfire.page. [Accessed 26 January 2016]

17. NavTech GPS. "Antcom Active L1/L2 Choke Ring Antenna." http://www.navtechgps.com/antcom_active_l1/l2_choke_ring_antenna_/. [Accessed 29 February 2016]

18. NGA/GPS Division. "NGA GPS Satellite Precise Ephemeris - Antenna Phase Center (APC)." http://earth-info.nga.mil/GandG/sathtml/APCexe.html. [Accessed 26 Oct 2015]

19. NovAtel. "DL-V3." http://www.NovAtel.com/assets/Documents/Papers/DL-V3.pdf. [Accessed 21 January 2016]

20. NovAtel. "Antennas Pinwheel OEM." http://www.novatel.com/assets/Documents/Papers/Pinwheel_OEM.pdf. [Accessed 29 February 2016]

21. Pilz, U., Gropengießer, W., Walder, F., Witt, J. & Werner, H. (2011). Quadcopter Localization Using RTK-GPS and Vision-Based Trajectory Tracking.. In S. Jeschke, H. Liu & D. Schilberg (eds.), ICIRA (1) (p./pp. 12-21), : Springer. ISBN: 978-3-642-25485-7

22. SBG Systems. "Ellipse Series." http://www.sbg-systems.com/docs/Ellipse_Series_ Leaflet.pdf. [Accessed 21 January 2016]

23. Stempfhuber, W. and M. Buchholz. "A Precise, Low-Cost RTK GNSS System for UAV Applications." Conference on Unmanned Aerial Vehicle in Geomatics, Zurich, Switzerland, 2011

24. Swift Navigation. "Piksi Datasheet v2.3.1." docs.swiftnav.com/pdfs/piksi_datasheet_v2.3.1.pdf. [Accessed 10 Oct 2015]

25. Rieke, M., T. Foerster, J. Geipel, and T. "Prinz High-Precision Positioning and Real-Time Data Processing of UAV- Systems," Conference on Unmanned Aerial Vehicle in Geomatics, Zurich, Switzerland, 2011

26. Raquet, John F. "Class Notes: EENG533 Navigation Using GPS". Winter Quarter, 2015, Air Force Institute of Technology, WPAFB, OH.

27. Spinelli, Christopher J. Development and Testing of a High-Speed Real Time Kinematic Precise DGPS Positioning System Between Two Aircraft. MS Thesis, AFIT/GCS/ENG/06-12. School of Electrical Engineering, Air Force Institute of Technology (AU), Wright-Patterson Air Force Base OH, September 2006 (A454831).

28. Teunissen, P. J. G., Jonge, P. J., & Tiberius, C. (1995). The LAMBDA-method for fast GPS surveying. GPS Technology Applications, (1), 8.

29. Tint, P., G. Tarmas, T. Koppel, K. Reinhold and S. Kalle. "Vibration and noise caused by lawn maintenance machines in association to risk to health," Biosystem Engineering Special Issue 1, 251-260, 2012.

# APPENDIX: CONFIGURATION SETTINGS

**Piksi Configuration**

| Configuration Setting | Base | Mobile |
|---|---|---|
| edge trigger | none | |
| antenna selection | External | |
| gpgsv msg rate | 10 | |
| gprmc msg rate | 10 | |
| gpvtg msg rate | 10 | |
| gpgll msg rate | 10 | |
| obs msg max size | 104 | |
| soln freq | 5 | |
| output every n obs | 1 | |
| dgnss solution mode | Low Latency* | |
| known baseline n | 0 | |
| known baseline e | 0 | |
| known baseline d | 0 | |
| broadcast | TRUE | FALSE |
| surveyed lat | 0 | |
| surveyed lon | 0 | |
| surveyed alt | 0 | |
| serial number | 9478 | 58856 |
| firmware version | v0.20 | |
| firmware built | Aug 4 2015 06:47:24 | |
| hw revision | piksi_2.3.1 | |
| nap version | v0.15 | |
| nap channels | 11 | |
| nap fft index bits | 13 | |
| heartbeat period milliseconds | 1000 | |
| watchdog | TRUE | |
| configuration string | AT&F;ATS1=115;<br>ATS2=128;<br>ATS5=0;<br>ATS16=65535;<br>ATS6=1;<br>ATS8=902000;<br>AT&W,ATZ | AT&F;ATS1=115;<br>ATS2=128;<br>ATS5=1;<br>ATS16=0;<br>ATS6=1;<br>ATS8=902000;<br>AT&W,ATZ |
| track cn0 threshold | 30 | |
| uart ftdi | | |
| mode | SBP | |

| | |
|---|---|
| sbp message mask | 65535 |
| baudrate | 1000000 |
| uart uarta | |
| mode | SBP |
| sbp message mask | 64 |
| configure telemetry radio on boot | TRUE |
| baud Rate | 115200 |
| uart uarta | |
| mode | SBP |
| sbp message mask | 65280 |
| configure telemetry radio on boot | TRUE |
| baud Rate | 115200 |

*dgnss solution mode was changed to ‘Time Matched’ for final Integration Test

## Pixhawk configuration

| Parameter | Value |
|---|---|
| EKF_GPS_TYPE | 0 |
| SERIAL1_BAUD | 115 |
| SERIAL1_PROTOCOL | 1 |
| SERIAL4_BAUD | 115 |
| SERIAL4_PROTOCOL | 5 |
| GPS_SBP_LOGMASK | -1 |
| GPS_TYPE | 1 |
| GPS_TYPE2 | 1 |

## Output Reliability Calculation

```
specified_rate=.2;                          %The inverse of the desired
                                            output frequency
delt=diff(sample_times);                    %Calculates the difference
                                            between each of the sample times
err=0;                                      %Initializes the count

for i=1:length(delt)                        %The for loop counts the number
    if delt(i)>specified_rate               of times the interval between
        err=err+1;                          two data points is greater than
    else                                    'specifed_rate'
        err=err;
    end
end

Output_reliability=(1-err/length(delt))*100
```

# REPORT DOCUMENTATION PAGE

*Form Approved*
*OMB No. 0704–0188*



| 1. REPORT DATE (DD–MM–YYYY) | 2. REPORT TYPE | 3. DATES COVERED *(From — To)* |
|---|---|---|
| 24-3-2016 | Master's Thesis | Sep 2014 – Mar 2016 |

**4. TITLE AND SUBTITLE**
The Efficacy of Implementing a Small, Low-Cost, Real Time Kinematic GPS System into a Small Unmanned Aerial System Architecture

5a. CONTRACT NUMBER
5b. GRANT NUMBER
5c. PROGRAM ELEMENT NUMBER

**6. AUTHOR(S)**
Hendricks, Kevin J., Captain, USAF

5d. PROJECT NUMBER
5e. TASK NUMBER
5f. WORK UNIT NUMBER

**7. PERFORMING ORGANIZATION NAME(S) AND ADDRESS(ES)**
Air Force Institute of Technology
Graduate School of Engineering and Management (AFIT/EN)
2950 Hobson Way
WPAFB OH 45433-7765

**8. PERFORMING ORGANIZATION REPORT NUMBER**
AFIT-ENV-MS-16-M-157

**9. SPONSORING / MONITORING AGENCY NAME(S) AND ADDRESS(ES)**
Air Force Research Lab - Aerospace Systems Directorate
Bldg 46
Wright-Patterson AFB OH 45433-7765
Paul A. Fleitz Jr., COMM 312-798-4628
Email: paul.fleitz@us.af.mil

10. SPONSOR/MONITOR'S ACRONYM(S)
AFRL/RQQC

11. SPONSOR/MONITOR'S REPORT NUMBER(S)

**12. DISTRIBUTION / AVAILABILITY STATEMENT**
DISTRIBUTION STATEMENT A: APPROVED FOR PUBLIC RELEASE; DISTRIBUTION UNLIMITED.

**13. SUPPLEMENTARY NOTES**


**14. ABSTRACT**
Along with the growing uses for small unmanned aerial systems (UAS) within the Department of Defense (DoD), is the utility of small UAS within the civilian market is also increasing. This has led to significant research and development on small UAS subsystems by the commercial market. The focus of this research is characterizing and investigating the application considerations of a small, low-cost real time kinematic (RTK) GPS receiver system. Work was also accomplished to characterize the accuracy and precision of the commonly used GPS receiver subsystem in small UAS to show the increased utility of the RTK GPS system. The results show that in a static environment, the RTK GPS system outperforms the commonly used standalone GPS receiver by a factor of 100 in two- and three-dimensional precision. However, the results from the tests involving a moving platform exposed several limitations which can degrade the precision of the RTK GPS system to precision values achievable by a standalone GPS receiver. These limitations do not inhibit the RTK GPS system's ability to perform its primary intended purpose, and can be mitigated through proper integration and application selection of the system. It is recommended that the Air Force Institute of Technology continue to use the investigated RTK GPS system as a ground truth source while proving other navigation technologies for UAS flight.

**15. SUBJECT TERMS**
Real-time Kinematics, RTK, DGPS, UAS, UAV

| 16. SECURITY CLASSIFICATION OF: | | | 17. LIMITATION OF ABSTRACT | 18. NUMBER OF PAGES | 19a. NAME OF RESPONSIBLE PERSON |
|---|---|---|---|---|---|
| a. REPORT U | b. ABSTRACT U | c. THIS PAGE U | UU | 111 | Dr. David R. Jacques, AFIT/ENV |
| | | | | | 19b. TELEPHONE NUMBER (Include Area Code) (937) 255 3636, x3329; david.jacques@afit.edu |